MODELING THE SYNCHROTRON: AN EXPLORATION OF DELAY-COUPLED NONLINEAR MATHIEU EQUATIONS

A Dissertation

Presented to the Faculty of the Graduate School

of Cornell University

in Partial Fulfillment of the Requirements for the Degree of

Doctor of Philosophy

by

Alexander Bernstein

August 2017

MODELING THE SYNCHROTRON:

AN EXPLORATION OF DELAY-COUPLED NONLINEAR MATHIEU EQUATIONS

Alexander Bernstein, Ph.D.

Cornell University 2017

A synchrotron is a circular particle accelerator where beams of electrons are maintained at high velocity. Each beam contains clusters of electrons called "bunches," and we model the vertical displacement of each bunch as simple harmonic motion with parametric excitation, i.e. the Mathieu equation. Different types of coupling are accounted for, including one that only takes effect after one orbit, which we model using delay terms; the resulting model is a system of delay-differential equations. Nonlinear and damping terms are also included to make the model more realistic and the dynamics more rich. Variations of this core model are examined using perturbation methods and checked against numerical integration.

BIOGRAPHICAL SKETCH

Alex Bernstein was born in New York state, although most of his childhood was spent in rural Connecticut. There he studied diligently in his coursework and spent his free time playing video games and attending martial arts classes. In high school he was a trumpet player in both marching band and jazz band, and he participated in various math competitions.

Alex went to college at Brandeis University in Massachusetts, where he initially considered a career in video game music composition before ultimately going through with a double major in math and physics. Finding neither to be completely satisfactory, he then went to study applied math at Cornell University, where he took a new interest in chess while completing his degree.

No one knows for sure what comes next. A tarot card reading predicted fame and fortune, but that reading is still under peer review.

This document is dedicated to the whimsical electron.

ACKNOWLEDGEMENTS

This work was only possible with the help and guidance of my advisor, Richard Rand. It's been a long journey, and he was there every step of the way.

I wish to thank my other committee members, Steven Strogatz and John Guckenheimer, for teaching me nonlinear dynamics and for reading my thesis. Their support has made me the mathematician I am today.

Another big thanks goes to Robert Meller, who introduced both Richard and myself to the world of particle accelerators. Without him, this document would be a completely different tale.

Thanks also to all family, friends, and faculty who have provided emotional support and helped me persevere. Although there are too many to list here, their anonymity belies the importance of their contribution to my success.

TABLE OF CONTENTS

LIST OF FIGURES

CHAPTER 1

INTRODUCTION: THE MODEL

There are two approaches when it comes to creating a mathematical model of some physical phenomenom. One approach is to build the model from the bottom up using first principles, such as quantum mechanics or thermodynamics. The other approach is to build the model from the top down, using mathematical considerations to capture observed behavior without regard for the underlying theory. The former approach tends to result in complicated models that require lots of computational power to simulate, whereas the latter tends to result in simpler models that are easier to analyze, but may be an approximation of reality.

The research presented here falls cleanly into the second category. Given the observed features of synchrotron dynamics, we designed a general model that captured these observations. Despite the simplicity of this approach, the general model was still too complicated to analyze in full. Instead, we used the general model as a basis for other, simpler models; as we gained deeper understanding of these simpler models, we were able to incorporate features of the general model to discover ever richer features.

1.1 The Model

The general model we analyze is a system of n nonlinear Mathieu equations:

$$\ddot{x}_1 + (\delta + \epsilon\cos t)x_1 + \epsilon\gamma x_1^3 + \epsilon\mu\dot{x}_1 = \epsilon\beta\sum_{j=1}^{n} x_j(t-T) \tag{1.1}$$

$$\ddot{x}_i + (\delta + \epsilon \cos t)x_i + \epsilon\gamma x_i^3 + \epsilon\mu\dot{x}_i \quad = \quad \epsilon\beta \sum_{j=1}^{n} x_j(t-T) + \epsilon\alpha x_{i-1} \quad , \quad 2 \leq \mathrm{i} \leq n \, (1.2)$$

This system of delay-differential equations is an example of a nonautonomous dynamical system. We are interested in describing changes in its behavior as parameters are varied, for example bifurcations which are associated with changes in the stability of the origin [13], [2].

Each chapter will introduce a variation of eqs. (1.1), (1.2) and use analytic techniques to analyze either the stability of the origin in linearized models or the amplitude of limit cycles in nonlinear models. The analytic results are then compared against numerical integration.

Since the Mathieu equation is a core part of this model, we offer a brief review of some of its most salient features.

1.1.1 Mathieu Equation

The Mathieu equation has been well studied [5], [12], [3]. In its most basic form, it consists of a linear spring with a variable coefficient:

$$\frac{d^2x}{dt^2} + (\delta + \epsilon \cos t)\, x = 0 \tag{1.3}$$

Here we assume that ϵ is small, and employ a perturbation technique known as two variable expansion [4], [10]. We set

$$\xi(t) = t, \quad \eta(t) = \epsilon t$$

where ξ is the time t and η is the slow time.

Since x is now a function of ξ and η, the derivative with respect to time t is expressed through the chain rule:

$$\dot{x} = x_\xi + \epsilon x_\eta$$

Similarly, for the second derivative we obtain:

$$\ddot{x} = x_{\xi\xi} + 2\epsilon x_{\xi\eta} + \epsilon^2 x_{\eta\eta}$$

We will only perturb up to $O(\epsilon)$, and so we will ignore the ϵ^2 terms.

We then expand x in a power series:

$$x(\xi, \eta) = x_0(\xi, \eta) + \epsilon x_1(\xi, \eta) + \cdots \tag{1.4}$$

Substituting (1.4) into (1.3) and collecting terms in ϵ, we arrive at the following equations:

$$x_{0,\xi\xi} + \delta x_0 = 0 \tag{1.5}$$

$$x_{1,\xi\xi} + \delta x_1 = -2x_{0,\xi\eta} - x_0 \cos\xi \tag{1.6}$$

The solution to (1.5) is simply:

$$x_0 = A(\eta)\cos\left(\sqrt{\delta}\xi\right) + B(\eta)\sin\left(\sqrt{\delta}\xi\right) \tag{1.7}$$

We then substitute (1.7) into (1.6) and apply some trigonometric identities to obtain:

$$\begin{aligned} x_{1,\xi\xi} + \delta x_1 &= 2\sqrt{\delta}\frac{dA}{d\eta}\sin\sqrt{\delta}\xi - 2\sqrt{\delta}\frac{dB}{d\eta}\cos\sqrt{\delta}\xi \\ &- \frac{A}{2}\left(\cos\left(\sqrt{\delta}+1\right)\xi + \cos\left(\sqrt{\delta}-1\right)\xi\right) \\ &- \frac{B}{2}\left(\sin\left(\sqrt{\delta}+1\right)\xi + \sin\left(\sqrt{\delta}-1\right)\xi\right) \end{aligned} \tag{1.8}$$

We want to choose A, B to eliminate resonances (also known as secular terms) in eq. (1.8). This results in a system of equations called the slow flow. For most values of δ this means we have:

$$\frac{dA}{d\eta} = 0, \qquad \frac{dB}{d\eta} = 0$$

Thus for general δ, the $\cos t$ driving term in eq. (1.3) has no effect on the dynamics.

However, if we choose $\delta = 1/4$, eq. (1.8) becomes:

$$\begin{aligned} x_{1,\xi\xi} + \delta x_1 &= \frac{dA}{d\eta}\sin\frac{\xi}{2} - \frac{dB}{d\eta}\cos\frac{\xi}{2} \\ &- \frac{A}{2}\left(\cos\frac{3\xi}{2} + \cos\frac{\xi}{2}\right) \\ &- \frac{B}{2}\left(\sin\frac{3\xi}{2} - \sin\frac{\xi}{2}\right) \end{aligned} \tag{1.9}$$

In this case, eliminating the secular terms results in the following slow flow:

$$\frac{dA}{d\eta} = -\frac{B}{2}, \qquad \frac{dB}{d\eta} = -\frac{A}{2} \quad \Rightarrow \quad \frac{d^2A}{d\eta^2} = \frac{A}{4} \tag{1.10}$$

Thus for this case the functions $A(\eta)$, $B(\eta)$ involve exponential growth, and so we say that $\delta = 1/4$ causes instability. In particular, this corresponds to a 2:1 subharmonic resonance in which the driving frequency is twice the natural frequency.

We can expand δ in a power series, known as "detuning" the resonance, to generalize these results:

$$\delta = \frac{1}{4} + \epsilon\delta_1 + \epsilon^2\delta_2 + \cdots \tag{1.11}$$

Substituting eq. (1.11) into eq. (1.3) produces an additional term in eq. (1.6):

$$x_{1,\xi\xi} + \delta x_1 = -2x_{0,\xi\eta} - x_0\cos\xi - \delta_1 x_0 \tag{1.12}$$

Following the same procedure as before, we end up with the following slow flow:

$$\frac{dA}{d\eta} = \left(\delta_1 - \frac{1}{2}\right), \quad \frac{dB}{d\eta} = -\left(\delta_1 + \frac{1}{2}\right) \quad \Rightarrow \quad \frac{d^2A}{d\eta^2} + \left(\delta_1^2 - \frac{1}{4}\right)A = 0 \tag{1.13}$$

For this case the functions $A(\eta)$, $B(\eta)$ involve exponential growth so long as $-1/2 < \delta_1 < 1/2$. For all other values of δ_1, $A(\eta)$, $B(\eta)$ are sine and cosine functions. In this way the value of δ_1 determines the stability of the system, and the change of stability occurs at the transition curves:

$$\delta = \frac{1}{4} \pm \frac{1}{2}\epsilon + O(\epsilon^2) \tag{1.14}$$

We call the region between the two curves a tongue of instability. Inside the tongue there is exponential growth, and outside the tongue there is sinusoidal growth. Figure 1.1 shows this tongue of instability.

It turns out that there are countably many tongues of instability for the Mathieu equation that emanate from the points $\delta = n^2/4$, and each one corresponds to a different kind of resonance. However, the research presented here focuses just on the 2:1 subharmonic resonance at $\delta = 1/4$ as that is the largest tongue of instability and thus the most significant one in practical applications.

Since our interest in eqs. (1.1), (1.2) comes from an application in the design of particle accelerators, we will briefly discuss this application in the next section.

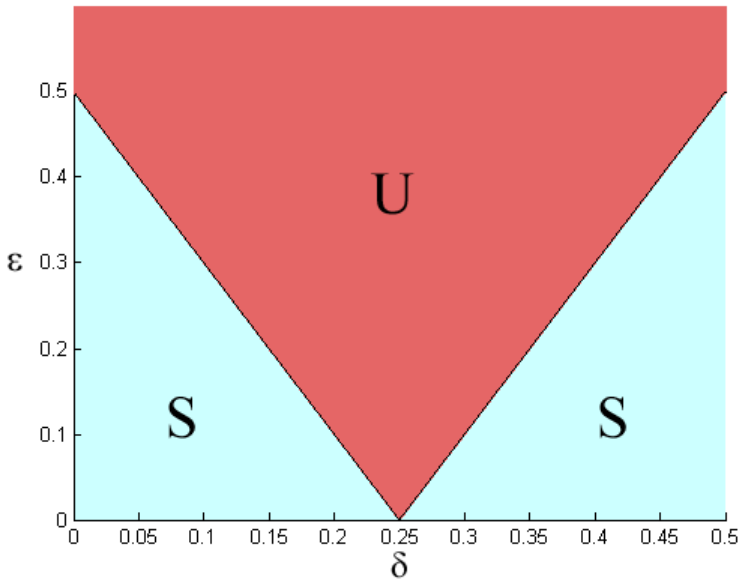

Figure 1.1: The tongue of instability that emanates from $\delta = \frac{1}{4}$ in the $\delta - \epsilon$ plane. The U represents the unstable region and the S represents the stable regions.

1.1.2 Application

The model was motivated by a novel application in particle physics, namely the dynamics of a generic circular particle accelerator [1].

The synchrotron is a particle accelerator in which a "particle" actually consists of a group of electrons called a "bunch," and the collection of all bunches is called a "train." We ignore the interactions of electrons inside each bunch and treat the entire bunch as a single particle.

Each bunch leaves an electrical disturbance behind it as it traverses around the synchrotron, and these wake fields are the main source of coupling in the model. The coupling is mediated by several sources, including ion coupling and the electron cloud effect.

Particle paths in the synchrotron are circle-like, but are not exact circles. Since the synchrotron lacks a central force, the circle-like particle orbits are achieved through the use of about 100 electromagnets spread around the periphery (see Figure 1.2).

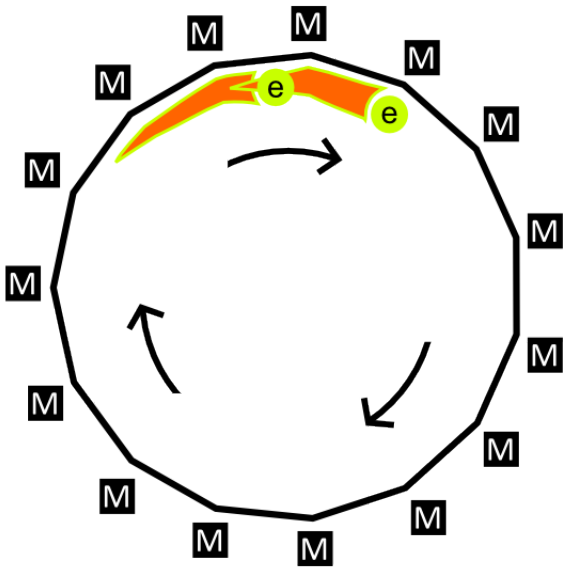

Figure 1.2: Two bunches moving clockwise along a polygonal path through the use of a system of electromagnets.

This means that the magnetic external forcing is periodic in rotation angle θ; assuming that the angular velocity of the bunch is constant with $\theta = \omega t$, the forcing is periodic in time as well. We can express this forcing function as a Fourier series, and we shall approximate this series by the first couple of terms in it, namely the constant term and the first cosine term.

We model each bunch as a scalar variable $x_i(t)$, $i = 1, \ldots, n$. Here x_i is the vertical displacement above equilibrium of the center of mass of the i^{th} bunch. Each x_i is modeled as a damped parametrically-forced oscillator, and we write:

$$\ddot{x}_1 + (\delta + \epsilon\cos t)x_1 + \epsilon\gamma x_1^3 + \epsilon\mu\dot{x}_1 = \epsilon\beta\sum_{j=1}^{n} x_j(t-T)$$

$$\ddot{x}_i + (\delta + \epsilon\cos t)x_i + \epsilon\gamma x_i^3 + \epsilon\mu\dot{x}_i = \epsilon\beta\sum_{j=1}^{n} x_j(t-T) + \epsilon\alpha x_{i-1} \quad , \quad 2 \leq \mathrm{i} \leq n$$

The nonlinear terms are included to create a more realistic model, since most natural phenomenon are nonlinear and linear models are a convenient approximation. The nonlinear parameter, γ, can be chosen to adjust the scale of the problem.

The damping terms are also included to create a more realistic model. The damping parameter, α, represents a multitude of physical phenomena and is chosen according to experimental observations.

The coupling terms on the right hand side may be modeled as consisting of two types [7]:

i) Plasma interactions
ii) Resistive wall coupling

In the case of plasma interactions, the radiation from a bunch produces an electron cloud which travels behind the bunch and influences the dynamics of the next bunch in the train. Since plasma interactions only persist for a very short time, we model this coupling as only affecting the next bunch in the train:

$$\alpha x_{i-1}$$

Physically, this coupling strength is affected by both the spacing between

bunches as well as the charge of each bunch, and α encapsulates both of those effects.

Resistive wall coupling arises from the finite conductivity of the beam pipe. The skin effect produces a long tail which may be modeled as a delay term, the duration of the delay being the transit time around the ring. The entire train can be modeled as a single superparticle with displacement equal to the train average, each bunch receiving the same force. This results in a coupling term of the form:

$$\beta \sum_{j=1}^{n} x_j(t - T)$$

where T =delay.

The simplest case is a single bunch, $n = 1$, in which we only consider the effect of delayed self-feedback:

$$\ddot{x} + (\delta + \epsilon \cos t)x = \beta x(t - T) \tag{1.15}$$

A system of this type has been investigated by Morrison and Rand [8]. It was shown that the region of instability associated with 2:1 subharmonic resonance can be eliminated by choosing the delay T appropriately.

CHAPTER 2

SCALING THE PERTURBATION PARAMETER

2.1 Introduction

The first variation of eqs. (1.1), (1.2) is incredibly simple, ignoring the effects of delay, nonlinear terms, and damping terms. We also limit our investigation to two bunches, as this is the smallest model to encapsulate all of the coupling effects. This simplicity provides a useful starting point by focusing on the difference between the two coupling terms.

However, a core question asked at this point is how to scale the perturbation parameter, ϵ, for each of the coupling terms. This is an important question in many perturbation problems because certain perturbation techniques will fail if the perturbation parameter is not chosen appropriately. Since the model used here is so simple, we opted to split it into two cases to investigate this aspect of perturbation theory.

The first model removes the ϵ terms from the coupling coefficients:

$$\ddot{x}_1 + (\delta + \epsilon \cos t)\, x_1 = \beta(x_1 + x_2) \tag{2.1}$$

$$\ddot{x}_2 + (\delta + \epsilon \cos t)\, x_2 = \beta(x_1 + x_2) + \alpha x_1 \tag{2.2}$$

The second model includes the ϵ terms for the coupling coefficients:

$$\ddot{x}_1 + (\delta + \epsilon \cos t)\, x_1 = \epsilon\beta(x_1 + x_2) \tag{2.3}$$

$$\ddot{x}_2 + (\delta + \epsilon \cos t)\, x_2 = \epsilon\beta(x_1 + x_2) + \epsilon\alpha x_1 \tag{2.4}$$

2.2 Model 1: Without ϵ

We start the analysis of eqs. (2.1), (2.2) by introducing a linear transformation to (u, v) coordinates:

$$x_1 = u + v, \qquad x_2 = \sqrt{\frac{\beta + \alpha}{\beta}}\,(u - v) \tag{2.5}$$

By applying this transformation to eqs. (2.1), (2.2) we obtain the following uncoupled equations:

$$\ddot{u} + (\Omega_u^2 + \epsilon \cos t)\, u = 0 \tag{2.6}$$

$$\ddot{v} + (\Omega_v^2 + \epsilon \cos t)\, v = 0 \tag{2.7}$$

where

$$\Omega_u^2 = \delta - \beta - \sqrt{\beta(\beta + \alpha)}$$

$$\Omega_v^2 = \delta - \beta + \sqrt{\beta(\beta + \alpha)}$$

The system has thus been reduced to a pair of uncoupled Mathieu equations, each of the form:

$$\ddot{z} + (\Delta + \epsilon \cos t)\, z = 0 \tag{2.8}$$

As is well known, this equation exhibits a 2:1 subharmonic resonance in the neighborhood of $\Delta = 1/4$. The boundaries of the associated tongue of instability are given by:

$$\Delta = \frac{1}{4} \pm \frac{\epsilon}{2} + O(\epsilon^2) \tag{2.9}$$

Comparison of eqs. (2.6), (2.7) with eq. (2.9) gives the instability tongues as $\Omega_i^2 = \frac{1}{4} \pm \frac{\epsilon}{2}$, or in terms of the parameter δ, the two tongues become:

$$\delta = \frac{1}{4} + \beta \pm \sqrt{\beta(\beta + \alpha)} \pm \frac{\epsilon}{2} + O(\epsilon^2) \tag{2.10}$$

If we write δ in the form $\delta = \delta_0 + \epsilon\delta_1 + O(\epsilon^2)$, we see that

$$\delta_0 = \frac{1}{4} + \beta \pm \sqrt{\beta(\beta + \alpha)} \tag{2.11}$$

$$\delta_1 = \pm\frac{1}{2} \tag{2.12}$$

It is clear from this result that the introduction of α and β only affects δ_0. Graphically, this means that as the parameters α, β change, the tongue of instability is translated left or right in the δ-ϵ plane, and the slopes of the transition curves remain the same.

Figure 2.1 shows the transition curves for different parameter values of α and β. The shaded regions are unstable and the unshaded regions are stable.

2.3 Model 2: With ϵ

For the second model, we will employ the technique of harmonic balance to find expressions for the transition curves to $O(\epsilon)$ [10]. We assume a solution can be found of the form:

$$x_1 = A\cos\frac{t}{2} + B\sin\frac{t}{2} \tag{2.13}$$

$$x_2 = C\cos\frac{t}{2} + D\sin\frac{t}{2} \tag{2.14}$$

We substitute these equations into eqs. (2.3), (2.4) and use some trigonometric identities to obtain:

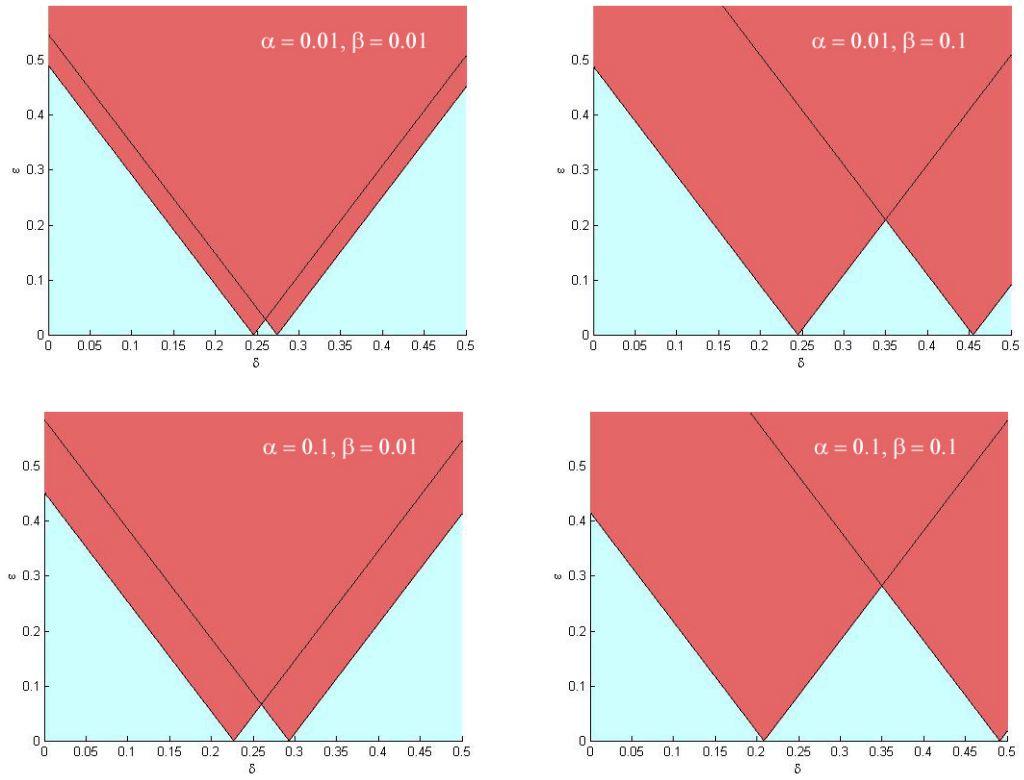

Figure 2.1: Effect of changing α, β for Model 1. Red regions are unstable and blue regions are stable.

$$
\begin{aligned}
0 &= \frac{\epsilon B}{2}\sin\frac{3t}{2} + \frac{\epsilon A}{2}\cos\frac{3t}{2} \\
&+ \left(B\delta - \epsilon\beta D - \epsilon\beta B - \frac{\epsilon B}{2} - \frac{B}{4}\right)\sin\frac{t}{2} \\
&+ \left(A\delta - \epsilon\beta C - \epsilon\beta A + \frac{\epsilon A}{2} - \frac{A}{4}\right)\cos\frac{t}{2}
\end{aligned}
$$

$$
\begin{aligned}
0 &= \frac{\epsilon D}{2}\sin\frac{3t}{2} + \frac{\epsilon C}{2}\cos\frac{3t}{2} \\
&+ \left(D\delta - \epsilon\beta D - \epsilon\beta B - \epsilon\alpha B - \frac{\epsilon D}{2} - \frac{D}{4}\right)\sin\frac{t}{2} \\
&+ \left(C\delta - \epsilon\beta C - \epsilon\beta A - \epsilon\alpha A + \frac{\epsilon C}{2} - \frac{C}{4}\right)\cos\frac{t}{2}
\end{aligned}
$$

Since we only care about $O(\epsilon)$ we disregard the $\cos\frac{3t}{2}$ and $\sin\frac{3t}{2}$ terms. Taking the coefficients of the remaining trigonometric functions to be zero, we obtain

four equations in A, B, C, and D. Writing this as a matrix, we get

$$\begin{bmatrix} -\frac{(4\beta-2)\epsilon-4\delta+1}{4} & 0 & -\epsilon\beta & 0 \\ -(\alpha+\beta)\epsilon & 0 & -\frac{(4\beta-2)\epsilon-4\delta+1}{4} & 0 \\ 0 & -\frac{(4\beta+2)\epsilon-4\delta+1}{4} & 0 & -\epsilon\beta \\ 0 & -(\alpha+\beta)\epsilon & 0 & -\frac{(4\beta+2)\epsilon-4\delta+1}{4} \end{bmatrix} \begin{bmatrix} A \\ B \\ C \\ D \end{bmatrix} = \begin{bmatrix} 0 \\ 0 \\ 0 \\ 0 \end{bmatrix} \tag{2.15}$$

For this system to have a nontrivial solution, the determinant must be zero. This produces the equation:

$$\begin{aligned} & - \frac{((4\beta-2)\epsilon-4\delta+1)^2\left(\frac{((4\beta+2)\epsilon-4\delta+1)^2}{16}-\beta(\alpha+\beta)\epsilon^2\right)}{16} \\ & + \beta(\alpha+\beta)\epsilon^2\left(\frac{((4\beta+2)\epsilon-4\delta+1)^2}{16}-\beta(\alpha+\beta)\epsilon^2\right)=0 \end{aligned} \tag{2.16}$$

This equation has the solution:

$$\delta = \frac{1}{4} + \epsilon\left(\beta \pm \sqrt{\beta(\beta+\alpha)} \pm \frac{1}{2}\right) + O(\epsilon^2) \tag{2.17}$$

As in Model 1, we write δ in the form $\delta = \delta_0 + \epsilon\delta_1 + O(\epsilon^2)$ to obtain

$$\delta_0 = \frac{1}{4} \tag{2.18}$$

$$\delta_1 = \beta \pm \sqrt{\beta(\beta+\alpha)} \pm \frac{1}{2} \tag{2.19}$$

Unlike in Model 1, here the introduction of α and β only affects δ_1. Graphically, this means that as the parameters α,β change, the tongue of instability narrows or widens while intersecting the same point on the δ-axis.

Figure 2.2 shows the transition curves for different parameter values of α and β. The shaded regions are unstable and the unshaded regions are stable.

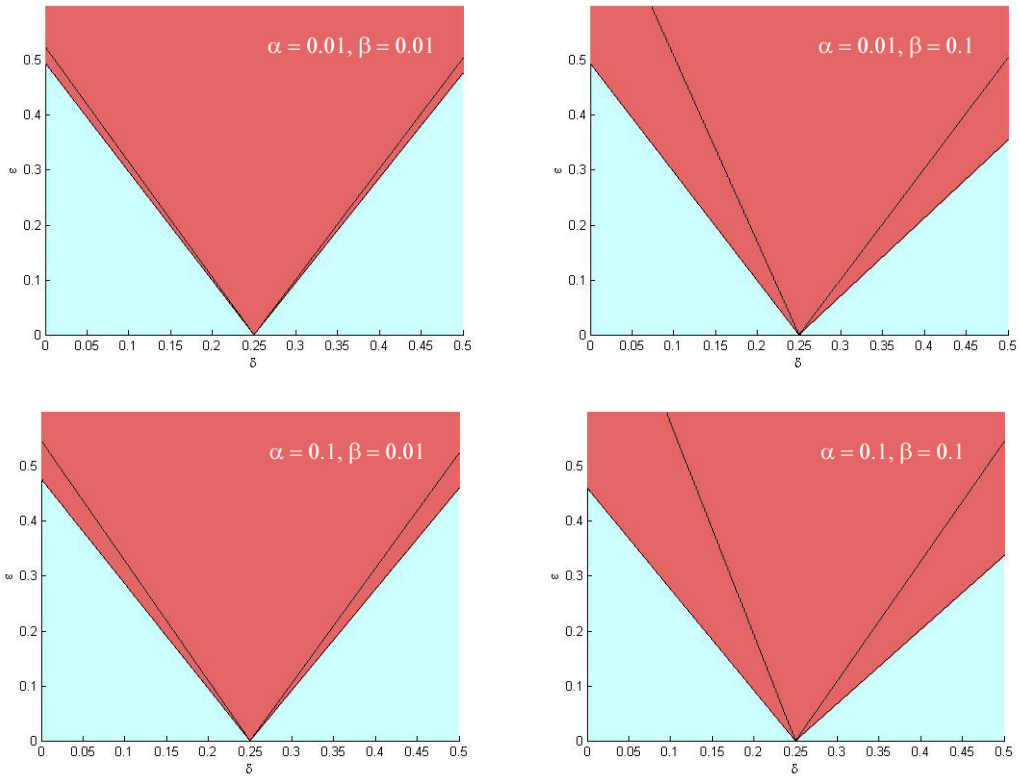

Figure 2.2: Effect of changing α, β for Model 2. Red regions are unstable and blue regions are stable.

2.4 Results

There are a few important observations to make about the tongues of instability.

2.4.1 Model 1

The first observation is that a small stable region appears between the tongues of instability, and it grows in size as both parameters α and β increase. Thus, while most of the graph becomes more unstable as the coupling increases, there is a region where the system actually becomes more stable.

The second observation to note is how these transition curves change with respect to both parameters. When β is increased, one of the tongues stays relatively still while the other tongue moves to the right. This causes the intersection of the tongues to move both up and to the right. When α is increased, the tongue on the left moves further to the left and the tongue on the right moves further to the right. This movement is balanced so that the intersection of the tongues moves straight up.

2.4.2 Model 2

Unlike in Model 1, there is no small stable region in Model 2 that grows in size with the parameters α, β. More explicitly, there is no region that becomes more stable as α and β are increased; all unstable regions stay unstable as the parameters increase.

2.5 Conclusion

In this chapter we showed the distinct effects that the two types of coupling, α and β, have on the system. Furthermore, we showed that both effects are relevant to the problem and are worth considering when mathematically modeling the synchrotron, and that the nature of the instability depends on the way in which the coupling is modeled.

Both models give the same result when ϵ is fixed and α, β vary. As an example, suppose $\epsilon = 0.1$ and we take $\alpha = \beta = 0.01$ in Model 1. Then the values of δ where the stability changes are given by $\delta_{crit} = (0.1957, 0.2958)$. For Model 2

we'd have to use the parameter values $\alpha = 0.1, \beta = 0.1$, since the coupling is $\epsilon\alpha$, $\epsilon\beta$ and $\epsilon = 0.1$. Using these values in Model 2 gives the same δ_{crit} values as the ones in Model 1. Figure 2.3 shows a graphical representation of this example.

The difference between these models comes when the parameters α, β are fixed and ϵ is allowed to vary.

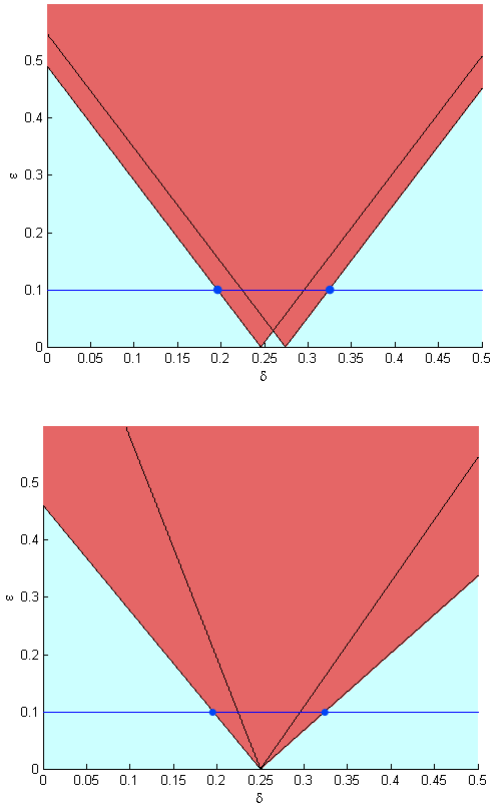

Figure 2.3: Comparison of the δ_{crit} values for both models when $\alpha = 0.01$, $\beta = 0.01$ in Model 1 (top) and $\alpha = 0.1$, $\beta = 0.1$ in Model 2 (bottom).

CHAPTER 3

THE EFFECT OF DELAY

3.1 Introduction

The second variation on eqs. (1.1), (1.2) includes delay and the damping term. However, nonlinear effects are still ignored as we only determine the stability of the origin, and the focus is still on only two bunches.

The model for this chapter is:

$$\ddot{x}_1 + (\delta + \epsilon\cos t)x_1 + \epsilon\mu\dot{x}_1 = \epsilon\beta\left(x_1(t-T) + x_2(t-T)\right) \tag{3.1}$$

$$\ddot{x}_2 + (\delta + \epsilon\cos t)x_2 + \epsilon\mu\dot{x}_2 = \epsilon\beta\left(x_1(t-T) + x_2(t-T)\right) + \epsilon\alpha x_1 \tag{3.2}$$

We start the analysis by applying a perturbation technique called two variable expansion.

3.2 Two Variable Expansion

We begin by transforming the system into a more tractable form. By using the linear transformation:

$$u = x_1 + x_2, \quad v = x_1 - x_2 \tag{3.3}$$

the system (3.1), (3.2) becomes

$$\ddot{u} + (\delta + \epsilon\cos t)u + \epsilon\mu\dot{u} = \frac{1}{2}\epsilon\alpha(u+v) + 2\epsilon\beta u_d \tag{3.4}$$

$$\ddot{v} + (\delta + \epsilon\cos t)v + \epsilon\mu\dot{v} = -\frac{1}{2}\epsilon\alpha(u+v) \tag{3.5}$$

where $u_d \equiv u(t-T)$.

In the special case when $\alpha = 0$ and $\mu = 0$, this system turns into an uncoupled system with one standard Mathieu equation and a Mathieu equation with delayed self feedback that's already been studied by Morrison and Rand [8]. Thus, the effect of α becomes clearer in the transformed system, and we have another established model for comparing our analytic results.

We use the two variable expansion method [4], [10] to study the dynamics of eqs. (3.4), (3.5). We set

$$\xi(t) = t, \quad \eta(t) = \epsilon t$$

where ξ is the time t and η is the slow time.

Since u and v are functions of ξ and η, the derivative with respect to time t is expressed through the chain rule:

$$\dot{u} = u_\xi + \epsilon u_\eta, \quad \dot{v} = v_\xi + \epsilon v_\eta$$

Similarly, for the second derivative we obtain:

$$\ddot{u} = u_{\xi\xi} + 2\epsilon u_{\xi\eta} + \epsilon^2 u_{\eta\eta}, \quad \ddot{v} = v_{\xi\xi} + 2\epsilon v_{\xi\eta} + \epsilon^2 v_{\eta\eta}$$

We will only perturb up to $O(\epsilon)$, and so we will ignore the ϵ^2 terms.

We then expand u and v in a power series in ϵ:

$$u(\xi,\eta) = u_0(\xi,\eta) + \epsilon u_1(\xi,\eta) + O(\epsilon^2), \quad v(\xi,\eta) = v_0(\xi,\eta) + \epsilon v_1(\xi,\eta) + O(\epsilon^2) \tag{3.6}$$

In addition, we detune off of the 2:1 subharmonic resonance by setting:

$$\delta = \frac{1}{4} + \epsilon\delta_1 + O(\epsilon^2) \tag{3.7}$$

Substituting (3.6), (3.7) into (3.4), (3.5) and collecting terms in ϵ, we arrive at the following equations:

$$u_{0,\xi\xi} + \frac{1}{4}u_0 = 0 \tag{3.8}$$

$$v_{0,\xi\xi} + \frac{1}{4}v_0 = 0 \tag{3.9}$$

$$u_{1,\xi\xi} + \frac{1}{4}u_1 = -2u_{0,\xi\eta} - \mu u_{0,\xi} - \delta_1 u_0 - u_0\cos\xi + \frac{\alpha}{2}(u_0 + v_0) + 2\beta u_{0_d} \tag{3.10}$$

$$v_{1,\xi\xi} + \frac{1}{4}v_1 = -2v_{0,\xi\eta} - \mu v_{0,\xi} - \delta_1 v_0 - v_0\cos\xi - \frac{\alpha}{2}(u_0 + v_0) \tag{3.11}$$

The solutions to (3.8) and (3.9) are simply:

$$u_0 = A(\eta)\cos\left(\frac{\xi}{2}\right) + B(\eta)\sin\left(\frac{\xi}{2}\right) \tag{3.12}$$

$$v_0 = C(\eta)\cos\left(\frac{\xi}{2}\right) + D(\eta)\sin\left(\frac{\xi}{2}\right) \tag{3.13}$$

We then substitute (3.12), (3.13) into (3.10), (3.11). Note that

$$u_{0_d} = A(\eta-\epsilon T)\cos\left(\frac{\xi}{2}-\frac{T}{2}\right) + B(\eta-\epsilon T)\sin\left(\frac{\xi}{2}-\frac{T}{2}\right) \tag{3.14}$$

Since ϵT is a small perturbation off η, we can approximate these delay terms as nondelay terms by expanding $A(\eta-\epsilon T)$ and $B(\eta-\epsilon T)$ in a Taylor series around η:

$$A(\eta-\epsilon T) = A(\eta) - \epsilon T A' + O(\epsilon^2) = A(\eta) + O(\epsilon) \tag{3.15}$$

Such a technique is common in the literature [8].

Trigonometrically expanding equation (3.14) gives terms in $\cos\frac{\xi}{2}$ and $\sin\frac{\xi}{2}$. The method involves setting the coefficients of such terms equal to zero in order to remove secular terms which cause resonance in equations (3.10), (3.11). This results in four equations in four unknowns:

$$A' = -\frac{\alpha D}{2} - 2\beta CB + \delta_1 B - \frac{\alpha B}{2} - \frac{B}{2} - 2\beta SA - \frac{\mu A}{2} \tag{3.16}$$

$$
\begin{aligned}
B' &= \frac{\alpha C}{2} - 2\beta \mathcal{S} B - \frac{\mu B}{2} + 2\beta C A - \delta_1 A + \frac{\alpha A}{2} - \frac{A}{2} && (3.17)\\
C' &= \delta_1 D + \frac{\alpha D}{2} - \frac{D}{2} - \frac{\mu C}{2} + \frac{\alpha B}{2} && (3.18)\\
D' &= -\frac{\mu D}{2} - \delta_1 C - \frac{\alpha C}{2} - \frac{C}{2} - \frac{\alpha A}{2} && (3.19)
\end{aligned}
$$

Where $\mathcal{S} = \sin\left(\frac{T}{2}\right), C = \cos\left(\frac{T}{2}\right)$.

The origin is an equilibrium point of the system, and its stability is determined by the coefficient matrix:

$$
\begin{bmatrix}
-\frac{4\beta\mathcal{S}+\mu}{2} & -\frac{4\beta C - 2\delta_1 + \alpha + 1}{2} & 0 & -\frac{\alpha}{2} \\
\frac{4\beta C - 2\delta_1 + \alpha - 1}{2} & -\frac{4\beta\mathcal{S}+\mu}{2} & \frac{\alpha}{2} & 0 \\
0 & \frac{\alpha}{2} & -\frac{\mu}{2} & \frac{2\delta_1 + \alpha - 1}{2} \\
-\frac{\alpha}{2} & 0 & -\frac{2\delta_1 + \alpha + 1}{2} & -\frac{\mu}{2}
\end{bmatrix} \qquad (3.20)
$$

The characteristic polynomial of this matrix is given by:

$$\lambda^4 + p\lambda^3 + q\lambda^2 + r\lambda + s = 0 \qquad (3.21)$$

where

$$p = 4\beta\mathcal{S} + 2\mu \qquad (3.22)$$

$$q = 4\beta^2\mathcal{S}^2 + 6\beta\mu\mathcal{S} + 4\beta^2 C^2 - 4\beta\delta_1 C + 2\alpha\beta C + \frac{3\mu^2}{2} + 2\delta_1^2 - \frac{1}{2} \qquad (3.23)$$

$$
\begin{aligned}
r &= 4\beta^2\mu\mathcal{S}^2 + 3\beta\mu^2\mathcal{S} + 4\beta\delta_1^2\mathcal{S} + 4\alpha\beta\delta_1\mathcal{S} \\
&- \beta\mathcal{S} + 4\beta^2\mu C^2 - 4\beta\delta_1\mu C + 2\alpha\beta\mu C + \frac{\mu^3}{2} + 2\delta_1^2\mu - \frac{\mu}{2} && (3.24)
\end{aligned}
$$

$$
\begin{aligned}
s &= \beta^2\mu^2\mathcal{S}^2 + 4\beta^2\delta_1^2\mathcal{S}^2 + 4\alpha\beta^2\delta_1\mathcal{S}^2 + \alpha^2\beta^2\mathcal{S}^2 - \beta^2\mathcal{S}^2 + \frac{\beta\mu^3\mathcal{S}}{2} \\
&+ 2\beta\delta_1^2\mu\mathcal{S} + 2\alpha\beta\delta_1\mu\mathcal{S} - \frac{\beta\mu\mathcal{S}}{2} + \beta^2\mu^2 C^2 + 4\beta^2\delta_1^2 C^2 + 4\alpha\beta^2\delta_1 C^2 \\
&+ \alpha^2\beta^2 C^2 - \beta^2 C^2 - \beta\delta_1\mu^2 C + \frac{\alpha\beta\mu^2 C}{2} - 4\beta\delta_1^3 C - 2\alpha\beta\delta_1^2 C + \beta\delta_1 C \\
&- \frac{\alpha\beta C}{2} + \frac{\mu^4}{16} + \frac{\delta_1^2\mu^2}{2} - \frac{\mu^2}{8} + \delta_1^4 - \frac{\delta_1^2}{2} + \frac{1}{16} && (3.25)
\end{aligned}
$$

We will use the Routh-Hurwitz Criterion on the polynomial (3.21) to determine the stability of the equilibrium point at the origin.

3.3 Routh-Hurwitz Criterion

In this work, by "linearly stable" we mean bounded in time, not to be confused with asymptotic stability which requires that the motion approaches the equilibrium point as $t \to \infty$. So for example, if a system has a pair of complex roots with negative real parts and a second pair of purely imaginary roots, we will say that this system is linearly stable.

The Routh-Hurwitz stability criterion [11] is a test on the coefficients of a characteristic polynomial to determine whether the system is linearly stable.

In Routh's original paper [11], he gives an example of a biquadratic polynomial that has the same form as (3.21). The conditions of stability are given by:

$$p > 0, \quad q > 0, \quad r > 0, \quad s > 0, \quad pqr - r^2 - p^2 s \geq 0$$

To obtain stability plots, we plot the curves $p = 0$, $q = 0$, $r = 0$, $s = 0$, and $pqr - r^2 - p^2 s = 0$, which partitions the $T - \delta_1$ plane into disjoint regions. Then we numerically evaluate the quantities p, q, r, and s at representative points in each region. Note that the resulting plots are 4π-periodic in T since the quantities p, q, r and s are 4π-periodic in T.

The first set of parameters we examined was $\mu = 0$, $\alpha = 0$, $\beta = 0.125$ (see Figure 3.1).

In the case when $\alpha = 0$ and $\mu = 0$, we see that the transformation (3.3) uncou-

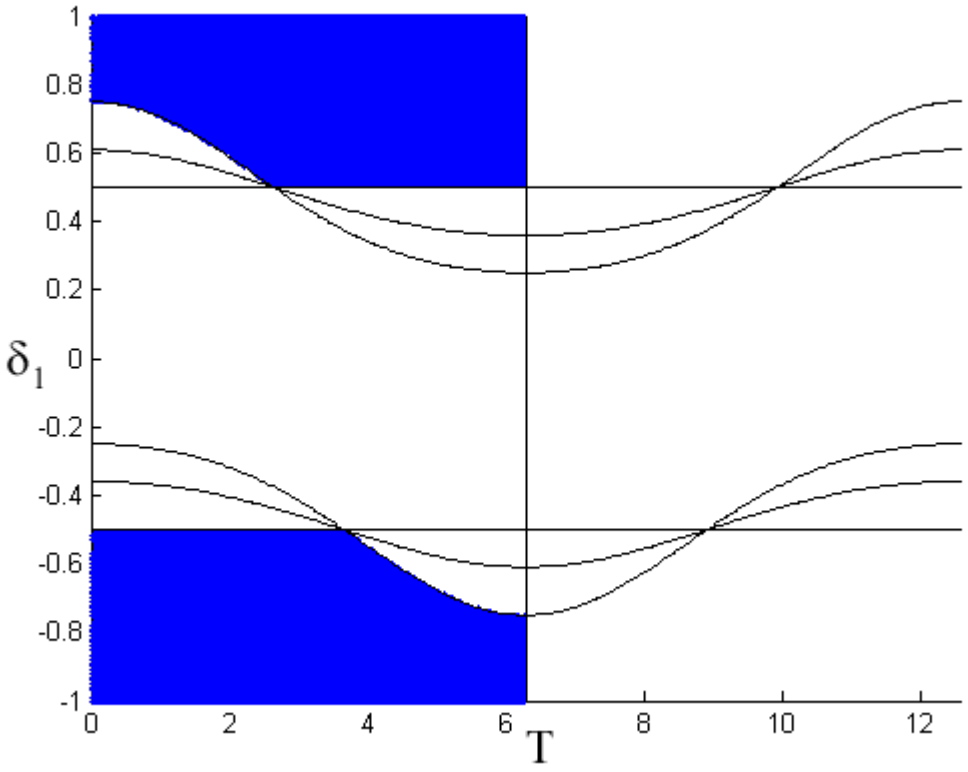

Figure 3.1: Plot of transition curves given by Routh-Hurwitz criterion for $\mu = 0$, $\alpha = 0$, and $\beta = 0.125$. The shaded regions are stable and the unshaded regions are unstable.

ples the system (3.1), (3.2) into a standard Mathieu equation (3.5) and a delayed Mathieu equation (3.4); the latter has been studied in [8]. For the system (3.1), (3.2) to be stable, both of eqs. (3.4), (3.5) must be stable. Since eq. (3.5) with $\alpha = 0$ does not involve delay, it causes instability in the region $|\delta - \frac{1}{4}| < \frac{\epsilon}{2} + O(\epsilon^2)$, or from eq. (3.7), in the horizontal strip $-0.5 < \delta_1 < 0.5$. See Figure 3.1, which agrees with these considerations and the results found in [8].

The next set of parameters we examined was $\mu = 0$, $\alpha = 0.01$, $\beta = 0.125$ (see Figure 3.2).

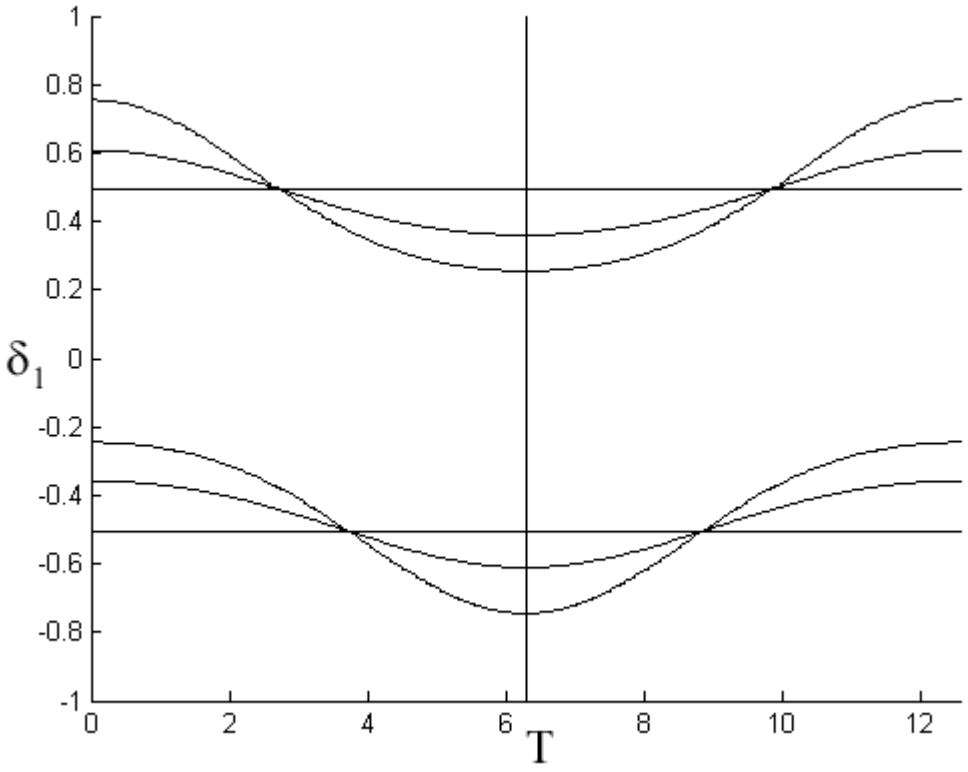

Figure 3.2: Plot of transition curves given by Routh-Hurwitz criterion for $\mu = 0$, $\alpha = 0.01$, and $\beta = 0.125$. The shaded regions are stable and the unshaded regions are unstable.

It turns out that, for any non-zero value of α (and $\mu = 0$), the Routh-Hurwitz criterion predicts instability almost everywhere! How is it possible that an arbitrarily small value of α can cause a discontinuous change in the stability diagram, from Figure 3.1 to Figure 3.2? The reason is that in the stable region of Fig. 3.1 there are purely imaginary eigenvalues λ, and an arbitrarily small value of α can move these eigenvalues to the right half plane.

A proof of the structural instability when $\mu = 0$ and $\alpha \neq 0$ can be found in the appendix.

The next set of parameters we examined was $\mu = 0.01$, $\alpha = 0.01$, $\beta = 0.125$ (see Figure 3.3).

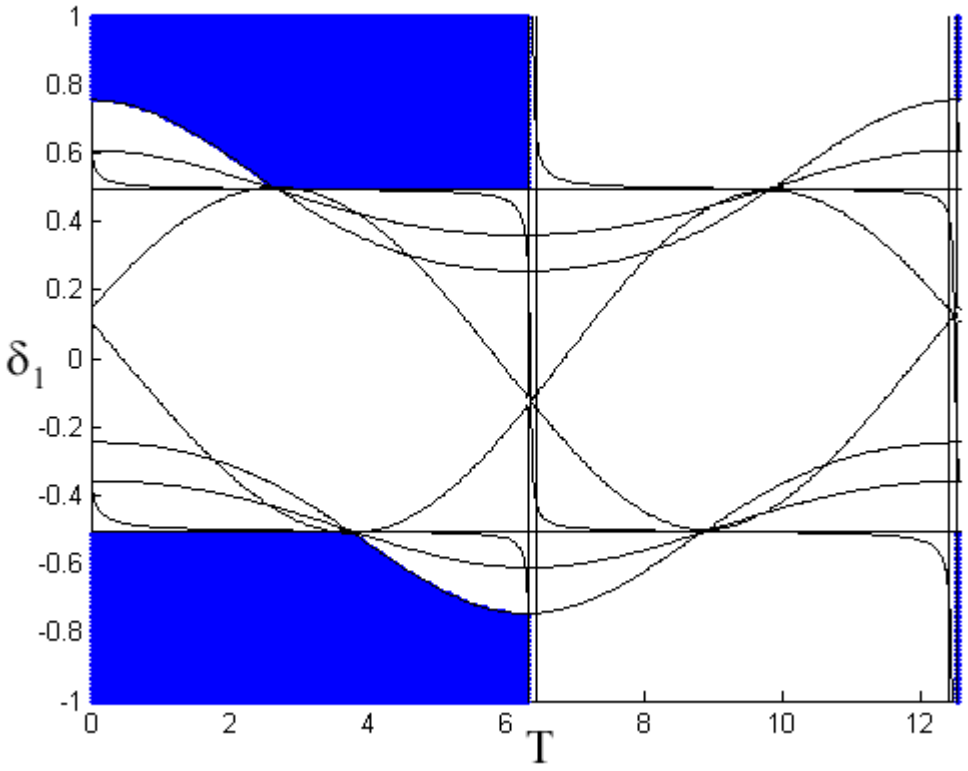

Figure 3.3: Plot of transition curves given by Routh-Hurwitz criterion for $\mu = 0.01$, $\alpha = 0.01$, and $\beta = 0.125$. The shaded regions are stable and the unshaded regions are unstable.

Figure 3.3 shows the effect of including nonzero damping to the system of Figure 3.2. We find that the stable regions from Figure 3.1 return. The introduction of μ also creates much more intricate potential transition curves, although as both α and μ are relatively small, the stable regions remain very similar to those in Fig. 3.1.

Note that the stability boundary at $T = 4\pi$ has moved slightly to the left.

The next set of parameters we examined was $\mu = 0.1$, $\alpha = 0.01$, $\beta = 0.125$ (see Figure 3.4).

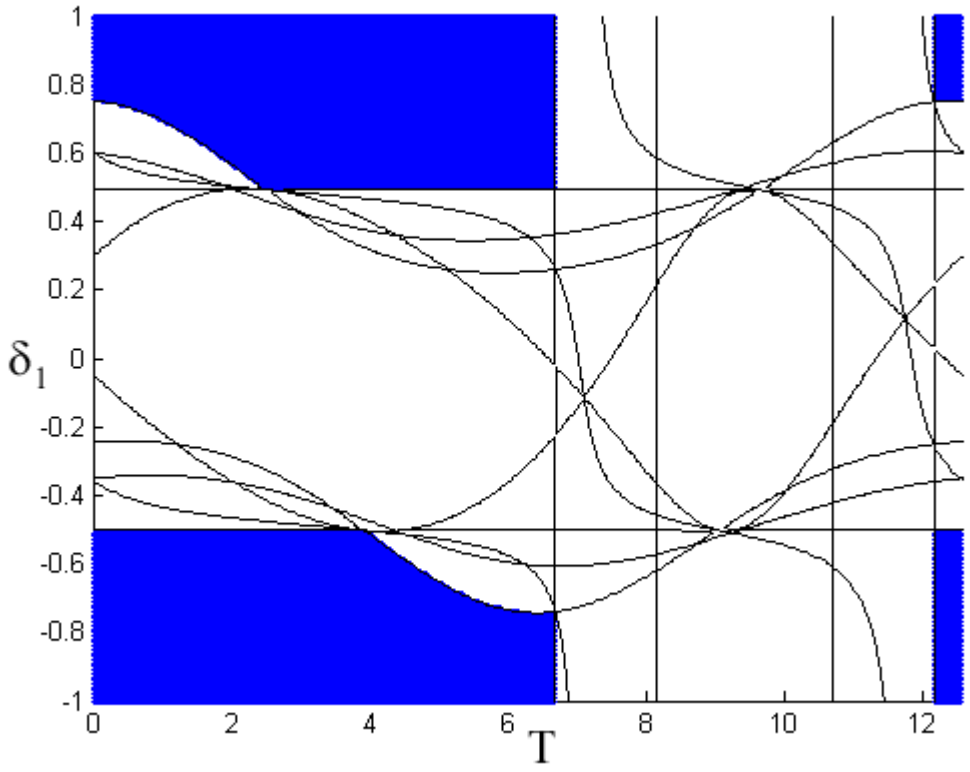

Figure 3.4: Plot of transition curves given by Routh-Hurwitz criterion for $\mu = 0.1$, $\alpha = 0.01$, and $\beta = 0.125$. The shaded regions are stable and the unshaded regions are unstable.

Here we can see that the effect of increasing μ is to increase the size of the stable region near $T = 2\pi$ and $T = 4\pi$. In particular, the stability boundary near $T = 4\pi$ that appeared in Figure 3.3 has moved further to the left, and the edge of the stable region around $T = 2\pi$ has moved to the right. These results reflect our intuition that adding damping increases the stability of the system.

The next set of parameters we examined was $\mu = 0.01$, $\alpha = 0.1$, $\beta = 0.125$ (see Figure 3.5).

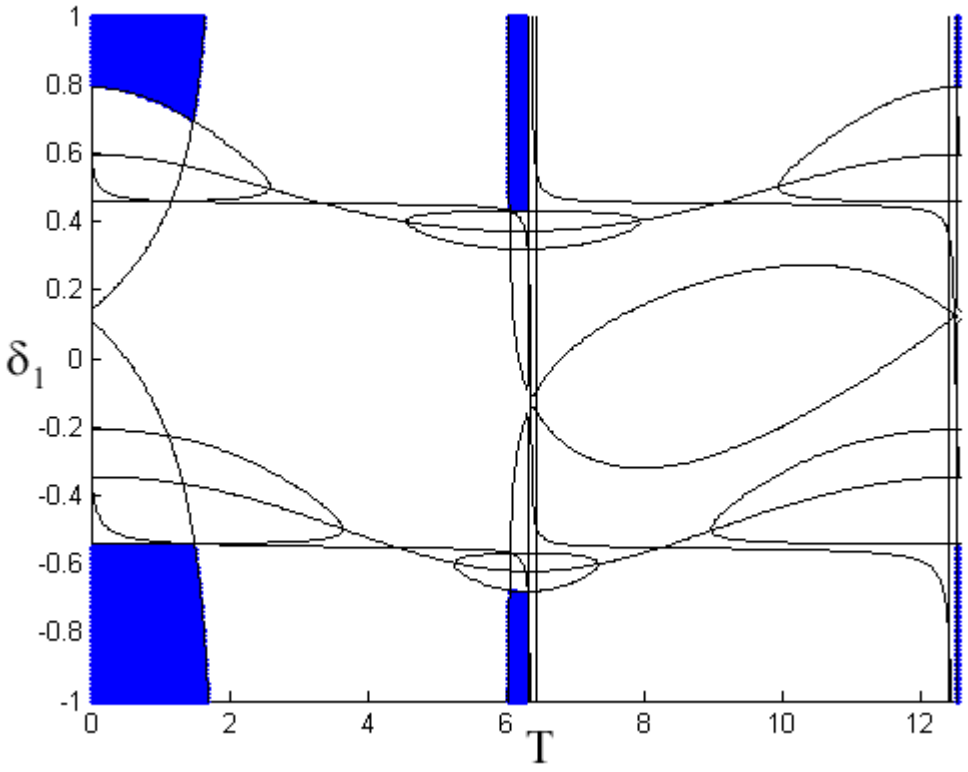

Figure 3.5: Plot of transition curves given by Routh-Hurwitz criterion for $\mu = 0.01$, $\alpha = 0.1$, and $\beta = 0.125$. The shaded regions are stable and the unshaded regions are unstable.

By comparing Fig. 3.3 with Fig. 3.5 we see that the effect of increasing α is to decrease the size of the stable region. The remaining stable regions cluster around $T = 0$ and $T = 2\pi$, suggesting that $T = n\pi$, $n = 0, 2, 4, \cdots$ produces stable regions that resist the destabilizing effect of the coupling term α.

We proceed to compare these results to numerical integration.

3.4 Numerical Results

The numerical computations use DDE23 in MATLAB [6] to numerically integrate the original DDE's (3.1), (3.2).

These numerical results will be compared to the analytical results presented earlier in the paper. We note that the analytical results are approximate due to a) the perturbation method, which truncates the solution, neglecting terms of $O(\epsilon^2)$, and b) the replacement of delay terms in the slow flow (3.16) - (3.19) by nondelay terms, a step which is valid for small ϵ. In this way both the numerical and the analytic approaches are approximate.

Determining the stability of this system via numerical integration is a challenge in and of itself. Specifically, in the limit as $\mu \to 0$, the system becomes Hamiltonian and there is no damping; in this case a stable solution is one that oscillates, rather than one that approaches a fixed point. Even when damping is present, the general effect of adding delay to the system is to increase the instability.

One of the ways to examine the growth of the system is by calculating the amplitude of the system as a function of time. In this work we measured the amplitude of the motion by computing $\sqrt{x_1(t)^2 + \dot{x}_1(t)^2 + x_2(t)^2 + \dot{x}_2(t)^2}$. In a stable system, the amplitude will either decrease or oscillate around a finite value. In an unstable system, the amplitude will increase without bound. Thus, a basic test for instability is to integrate over a long time period and compare the amplitude at the final time with the amplitude at an earlier time. In particular we compared the amplitude at time 6000 with the amplitude at time 5000. In all computations we used $\epsilon = 0.01$.

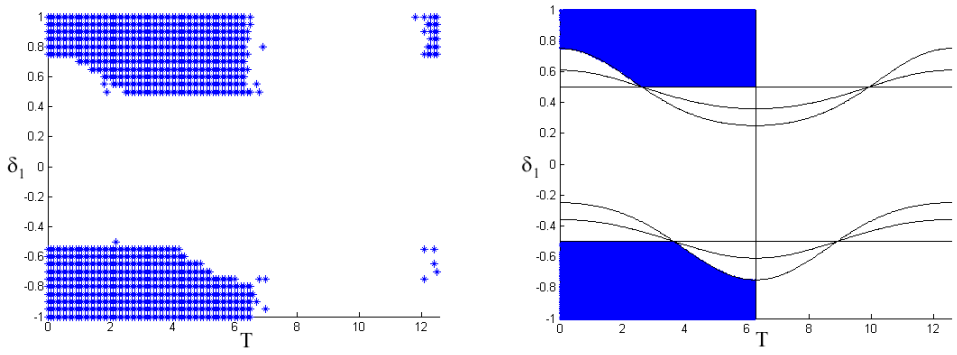

Figure 3.6: Comparison of analytic results with numerical integration for $\mu = 0$, $\alpha = 0$, and $\beta = 0.125$. The left graph is the result of the numerical integration. The right graph is Figure 3.1.

In Figure 3.6 we see that for $\alpha = 0$ and $\mu = 0$ the numerical results closely match the perturbation results. The numerical results for $\alpha = 0.01, \mu = 0.01$ and $\alpha = 0.01, \mu = 0.1$ are also quite similar to their corresponding results from the Routh-Hurwitz criterion (Figure 3.3 and Figure 3.4) and so we do not show them again here.

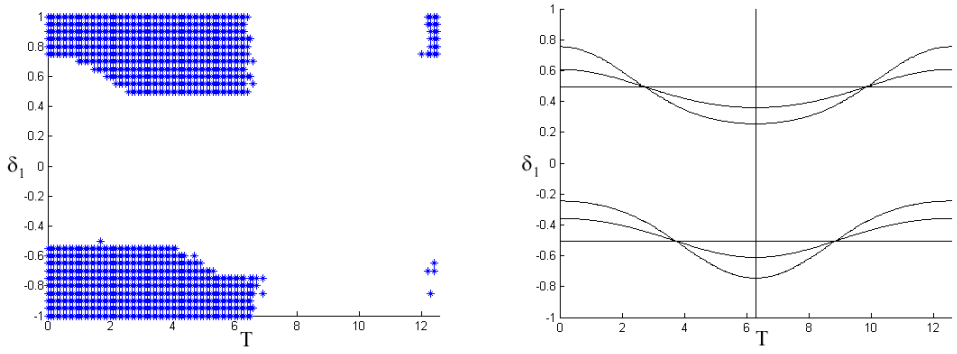

Figure 3.7: Comparison of analytic results with numerical integration for $\mu = 0$, $\alpha = 0.01$, and $\beta = 0.125$. The left graph is the result of the numerical integration. The right graph is Figure 3.2.

In Figure 3.7 we see that in the case when α is nonzero and μ is zero the numerical results differ quite strongly from the results predicted by the Routh-

Hurwitz criterion. Recall from Figure 3.2 that the introduction of small α caused instability almost everywhere due to the occurrence of purely imaginary roots in the $\alpha = 0$, $\mu = 0$ case. We believe the failure of the numerical solution to match the analytic solution in Figure 3.7 is because the numerical solver is inadvertently adding a small bit of damping to the system due to numerical error.

To estimate the quantity of inherent damping in the numerical solution, we inserted negative values for the damping coefficient μ and adjusted the size of μ so that analytic and numerical results agree. For example, in the case of Fig. 3.7, we set $\mu = -0.2$ in the numerical results, producing agreement between numerical and analytic results as can be seen in Figure 3.8.

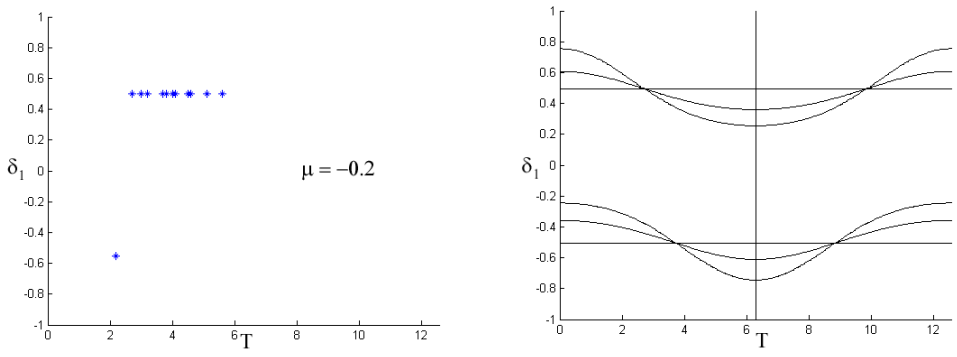

Figure 3.8: Comparison of analytic results with numerical integration for $\alpha = 0.01$ and $\beta = 0.125$. The left graph is the result of the numerical integration with an adjusted μ value of $\mu = -0.2$. The right graph is Figure 3.2 with $\mu = 0$.

In Figure 3.9 we see that when α is greater than μ the numerical results and perturbation results do not match. However, in Figure 3.10 we see that for an adjusted μ value of $\mu = -0.0375$ the numerical results more closely match the Routh-Hurwitz results. This outcome is important as it highlights that the inherent damping of the numerical integrator depends on α.

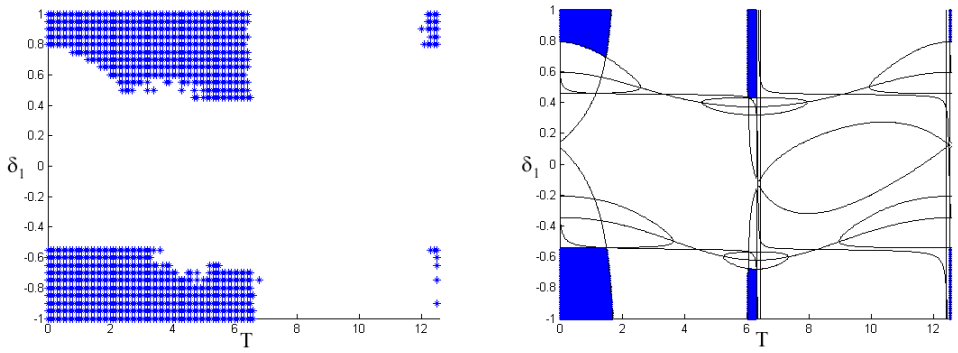

Figure 3.9: Comparison of analytic results with numerical integration for $\mu = 0.01$, $\alpha = 0.1$, and $\beta = 0.125$. The left graph is the result of the numerical integration. The right graph is Figure 3.5.

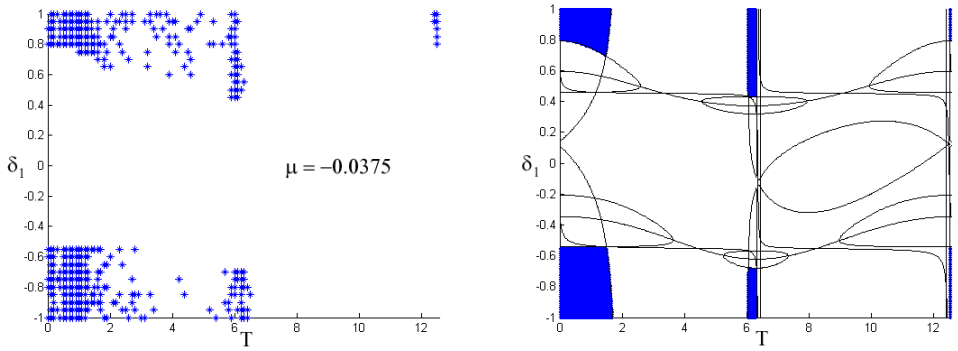

Figure 3.10: Comparison of analytic results with numerical integration for $\alpha = 0.1$ and $\beta = 0.125$. The left graph is the result of the numerical integration with an adjusted μ value of $\mu = -0.0375$. The right graph is Figure 3.5 with $\mu = 0.01$.

Note that adjusted numerical results show several scattered stable points in regions that are predicted to be unstable. This is not an artifact of the μ adjustment but rather is due to the inaccuracy of the numerical method. The results become more accurate as the numerical integrator runs for longer times. In particular, for Figures 3.9 and 3.10 we compared the amplitude after 8000 time steps with the amplitude after 6000 time steps.

3.5 Conclusion

In this chapter, we investigated the dynamics of two coupled Mathieu equations with delay. In particular we analyzed the stability of the origin and the effect of delay and damping on stability. We used the method of two variable expansion to calculate a characteristic polynomial of the system's slow flow, and used the Routh-Hurwitz criterion to determine stability; these results were then compared with numerical integration.

The numerical results closely matched the Routh-Hurwitz criterion when both $\alpha = 0$ and $\mu = 0$, but introducing nonzero values of either of these parameters caused the two methods to yield very different results. We believe this is because the numerical solver implicitly carries its own damping effect. By comparing perturbation results with those of numerical integration we were able to estimate the extent of inherent damping in the numerical integrator DDE23 in MATLAB.

In the parameter range which we explored, we found that increases in α and delay T tended to decrease stability, whereas an increase in damping μ tended to raise stability.

CHAPTER 4

THE EFFECT OF DELAY 2: A BETTER APPROACH

4.1 Introduction

The third variation on eqs. (1.1), (1.2) extends the results of the previous chapter by considering an alternative to using the approximation (3.15) that provides more accurate analytic results. This model is therefore very similar to the last model, although we do include the nonlinear term this time.

The model for this chapter is:

$$\ddot{x}_1 + (\delta + \epsilon\cos t)x_1 + \epsilon\gamma x_1^3 + \epsilon\mu\dot{x}_1 = \epsilon\beta\left(x_1(t-T) + x_2(t-T)\right) \tag{4.1}$$

$$\ddot{x}_2 + (\delta + \epsilon\cos t)x_2 + \epsilon\gamma x_2^3 + \epsilon\mu\dot{x}_2 = \epsilon\beta\left(x_1(t-T) + x_2(t-T)\right) + \epsilon\alpha x_1 \tag{4.2}$$

As in the last chapter, we start the analysis by applying a perturbation technique called two variable expansion.

4.2 Two Variable Expansion

We use the two variable expansion method [4], [10] to study the dynamics of eqs. (4.1), (4.2). We set

$$\xi(t) = t, \quad \eta(t) = \epsilon t$$

where ξ is the time t and η is the slow time.

Since x_1 and x_2 are functions of ξ and η, the derivative with respect to time t

is expressed through the chain rule:

$$\dot{x}_1 = x_{1_\xi} + \epsilon x_{1_\eta}, \quad \dot{x}_2 = x_{2_\xi} + \epsilon x_{2_\eta}$$

Similarly, for the second derivative we obtain:

$$\ddot{x}_1 = x_{1_{\xi\xi}} + 2\epsilon x_{1_{\xi\eta}} + \epsilon^2 x_{1_{\eta\eta}}, \quad \ddot{x}_2 = x_{2_{\xi\xi}} + 2\epsilon x_{2_{\xi\eta}} + \epsilon^2 x_{2_{\eta\eta}}$$

We will only perturb up to $O(\epsilon)$, and so we will ignore the ϵ^2 terms.

We then expand x_1 and x_2 in a power series in ϵ:

$$x_1(\xi,\eta) = x_{1_0}(\xi,\eta) + \epsilon x_{1_1}(\xi,\eta) + O(\epsilon^2), \quad x_2(\xi,\eta) = x_{2_0}(\xi,\eta) + \epsilon x_{2_1}(\xi,\eta) + O(\epsilon^2) \tag{4.3}$$

In addition, we detune off of the 2:1 subharmonic resonance by setting:

$$\delta = \frac{1}{4} + \epsilon\delta_1 + O(\epsilon^2) \tag{4.4}$$

Substituting (4.3), (4.4) into (4.1), (4.2) and collecting terms in ϵ, we arrive at the following equations:

$$\begin{aligned}
x_{1_{0,\xi\xi}} + \frac{1}{4}x_{1_0} &= 0 && (4.5)\\
x_{2_{0,\xi\xi}} + \frac{1}{4}x_{2_0} &= 0 && (4.6)\\
x_{1_{1,\xi\xi}} + \frac{1}{4}x_{1_1} &= -2x_{1_{0,\xi\eta}} - \gamma x_{1_0}^3 - \mu x_{1_{0,\xi}} - \delta_1 x_{1_0} - x_{1_0}\cos\xi \\
&\quad + \beta(x_{1_0}(t-T) + x_{2_0}(t-T)) && (4.7)\\
x_{2_{1,\xi\xi}} + \frac{1}{4}x_{2_1} &= -2x_{2_{0,\xi\eta}} - \gamma x_{2_0}^3 - \mu x_{2_{0,\xi}} - \delta_1 x_{2_0} - x_{2_0}\cos\xi \\
&\quad + \beta(x_{1_0}(t-T) + x_{2_0}(t-T)) + \alpha x_{1_0} && (4.8)
\end{aligned}$$

The solutions to (4.5) and (4.6) are simply:

$$\begin{aligned}
x_{1_0} &= A_1(\eta)\cos\left(\frac{\xi}{2}\right) + B_1(\eta)\sin\left(\frac{\xi}{2}\right) && (4.9)\\
x_{2_0} &= A_2(\eta)\cos\left(\frac{\xi}{2}\right) + B_2(\eta)\sin\left(\frac{\xi}{2}\right) && (4.10)
\end{aligned}$$

We then substitute (4.9), (4.10) into (4.7), (4.8). Note that:

$$x_{1_0}(t-T) = A_1(\eta-\epsilon T)\cos\left(\frac{\xi}{2}-\frac{T}{2}\right)+B_1(\eta-\epsilon T)\sin\left(\frac{\xi}{2}-\frac{T}{2}\right) \tag{4.11}$$

$$x_{2_0}(t-T) = A_2(\eta-\epsilon T)\cos\left(\frac{\xi}{2}-\frac{T}{2}\right)+B_2(\eta-\epsilon T)\sin\left(\frac{\xi}{2}-\frac{T}{2}\right) \tag{4.12}$$

Using trigonometric identities, these equations can be written in terms of $\cos\frac{\xi}{2}$ and $\sin\frac{\xi}{2}$. We set the coefficients of such terms equal to zero in order to remove the secular terms and avoid resonance. This results in four delay-differential equations in four unknowns:

$$\begin{aligned} A_1' &= -\beta\sin\left(\frac{T}{2}\right)(A_{1_d}+A_{2_d})-\beta\cos\left(\frac{T}{2}\right)(B_{1_d}+B_{2_d}) \\ &- \frac{\mu}{2}A_1+\left(\delta_1-\frac{1}{2}\right)B_1+\frac{3\gamma B_1}{4}\left(A_1^2+B_1^2\right) \end{aligned} \tag{4.13}$$

$$\begin{aligned} B_1' &= -\beta\sin\left(\frac{T}{2}\right)(B_{1_d}+B_{2_d})+\beta\cos\left(\frac{T}{2}\right)(A_{1_d}+A_{2_d}) \\ &- \frac{\mu}{2}B_1-\left(\delta_1+\frac{1}{2}\right)A_1-\frac{3\gamma A_1}{4}\left(A_1^2+B_1^2\right) \end{aligned} \tag{4.14}$$

$$\begin{aligned} A_2' &= -\beta\sin\left(\frac{T}{2}\right)(A_{1_d}+A_{2_d})-\beta\cos\left(\frac{T}{2}\right)(B_{1_d}+B_{2_d}) \\ &- \frac{\mu}{2}A_2+\left(\delta_1-\frac{1}{2}\right)B_2+\frac{3\gamma B_2}{4}\left(A_2^2+B_2^2\right)-\alpha B_1 \end{aligned} \tag{4.15}$$

$$\begin{aligned} B_2' &= -\beta\sin\left(\frac{T}{2}\right)(B_{1_d}+B_{2_d})+\beta\cos\left(\frac{T}{2}\right)(A_{1_d}+A_{2_d}) \\ &- \frac{\mu}{2}B_2-\left(\delta_1+\frac{1}{2}\right)A_2-\frac{3\gamma A_2}{4}\left(A_2^2+B_2^2\right)+\alpha A_1 \end{aligned} \tag{4.16}$$

Where $A_{1_d} \equiv A_1(t-T)$, $B_{1_d} \equiv B_1(t-T)$ etc.

In the previous chapter we employed the following approximation here:

$$A_d = A(\eta-\epsilon T) = A(\eta)-\epsilon T A'+O(\epsilon^2) = A(\eta)+O(\epsilon)$$

We will briefly go over this case in the next section to demonstrate that we get the same results that we could using the Routh-Hurwitz criterion, although

the main point of this chapter is to keep the delay terms A_{1_d}, B_{1_d}, A_{2_d}, B_{2_d} in the slow flow and observe the difference in slow flow dynamics.

4.3 Analytic Results

The present authors are interested in analyzing the stability of the origin of the original system (4.1), (4.2), which also corresponds to the origin of the slow flow (4.13), (4.14), (4.15), (4.16). To help accomplish this goal, we will linearize the slow flow around the origin and analyze the stability of that system, since the stability of the linearized system will be the same as the stability of the nonlinear system.

Thus, the slow flow becomes:

$$\begin{aligned} A_1' &= -\beta \sin\left(\frac{T}{2}\right)(A_{1_d} + A_{2_d}) - \beta \cos\left(\frac{T}{2}\right)(B_{1_d} + B_{2_d}) \\ &- \frac{\mu}{2}A_1 + \left(\delta_1 - \frac{1}{2}\right)B_1 \end{aligned} \tag{4.17}$$

$$\begin{aligned} B_1' &= -\beta \sin\left(\frac{T}{2}\right)(B_{1_d} + B_{2_d}) + \beta \cos\left(\frac{T}{2}\right)(A_{1_d} + A_{2_d}) \\ &- \frac{\mu}{2}B_1 - \left(\delta_1 + \frac{1}{2}\right)A_1 \end{aligned} \tag{4.18}$$

$$\begin{aligned} A_2' &= -\beta \sin\left(\frac{T}{2}\right)(A_{1_d} + A_{2_d}) - \beta \cos\left(\frac{T}{2}\right)(B_{1_d} + B_{2_d}) \\ &- \frac{\mu}{2}A_2 + \left(\delta_1 - \frac{1}{2}\right)B_2 - \alpha B_1 \end{aligned} \tag{4.19}$$

$$\begin{aligned} B_2' &= -\beta \sin\left(\frac{T}{2}\right)(B_{1_d} + B_{2_d}) + \beta \cos\left(\frac{T}{2}\right)(A_{1_d} + A_{2_d}) \\ &- \frac{\mu}{2}B_2 - \left(\delta_1 + \frac{1}{2}\right)A_2 + \alpha A_1 \end{aligned} \tag{4.20}$$

As eqs. (4.17), (4.18), (4.19), (4.20) are linear in A_1, B_1, A_2, and B_2, we know that the general solution will be a linear combination of exponential functions.

Thus, for instance, $A_1 = C_1 e^{\lambda\eta}$ and its derivative becomes:

$$A_1' = \frac{\mathrm{d}}{\mathrm{d}\eta}\left(C_1 e^{\lambda\eta}\right) = C_1 \lambda e^{\lambda\eta}$$

In addition, the delay term becomes:

$$A_{1_d} = A_1(\eta - \epsilon T) = C_1 e^{\lambda\eta - \epsilon\lambda T} = C_1 e^{\lambda\eta} e^{-\epsilon\lambda T} = A_1 e^{-\epsilon\lambda T}$$

Substituting these expressions into eqs. (4.17), (4.18), (4.19), (4.20) and expressing the system in matrix form, we obtain:

$$\begin{bmatrix} -\beta\nu\mathcal{S} - \frac{\mu}{2} - \lambda & -\beta\nu\mathcal{C} + \delta_1 - \frac{1}{2} & -\beta\nu\mathcal{S} & -\beta\nu\mathcal{C} \\ \beta\nu\mathcal{C} - \delta_1 - \frac{1}{2} & -\beta\nu\mathcal{S} - \frac{\mu}{2} - \lambda & \beta\nu\mathcal{C} & -\beta\nu\mathcal{S} \\ -\beta\nu\mathcal{S} & -\beta\nu\mathcal{C} - \alpha & -\beta\nu\mathcal{S} - \frac{\mu}{2} - \lambda & -\beta\nu\mathcal{C} + \delta_1 - \frac{1}{2} \\ \beta\nu\mathcal{C} + \alpha & -\beta\nu\mathcal{S} & \beta\nu\mathcal{C} - \delta_1 - \frac{1}{2} & -\beta\nu\mathcal{S} - \frac{\mu}{2} - \lambda \end{bmatrix} \begin{bmatrix} C_1 \\ C_2 \\ C_3 \\ C_4 \end{bmatrix} = \begin{bmatrix} 0 \\ 0 \\ 0 \\ 0 \end{bmatrix} \tag{4.21}$$

Where $\mathcal{S} = \sin\left(\frac{T}{2}\right), \mathcal{C} = \cos\left(\frac{T}{2}\right), \nu = e^{-\epsilon\lambda T}$.

Our goal is to compare two approaches: 1) Replacing delay terms by nondelay terms, e.g. A_d by A, versus 2) Analyzing the system with the delay terms. Replacing delayed terms with nondelay terms is equivalent to setting $\nu = 1$, and this can be achieved by setting $\epsilon = 0$ or $\lambda = 0$ in the slow flow.

To obtain nontrivial solutions we set the determinant of this matrix equal to zero, resulting in a characteristic equation of the form:

$$\lambda^4 + p\lambda^3 + q\lambda^2 + r\lambda + s = 0 \tag{4.22}$$

Where

$$p = 4\beta\nu\mathcal{S} + 2\mu \tag{4.23}$$

$$q = 6\beta\mu\nu\mathcal{S} - 4\beta\delta_1\nu\mathcal{C} + 2\alpha\beta\nu\mathcal{C} + 4\beta^2\nu^2 + \frac{3\mu^2}{2} + 2\delta_1^2 - \frac{1}{2} \tag{4.24}$$

$$\begin{aligned} r &= 4\beta\delta_1^2\nu\mathcal{S} + 4\alpha\beta\delta_1\nu\mathcal{S} + 3\beta\mu^2\nu\mathcal{S} - \beta\nu\mathcal{S} - 4\beta\delta_1\mu\nu\mathcal{C} \\ &+ 2\alpha\beta\mu\nu\mathcal{C} + 4\beta^2\mu\nu^2 + \frac{\mu^3}{2} + 2\delta_1^2\mu - \frac{\mu}{2} \end{aligned} \tag{4.25}$$

$$\begin{aligned} s &= 2\beta\delta_1^2\mu\nu\mathcal{S} + 2\alpha\beta\delta_1\mu\nu\mathcal{S} + \frac{\beta\mu^3\nu\mathcal{S}}{2} - \frac{\beta\mu\nu\mathcal{S}}{2} - 4\beta\delta_1^3\nu\mathcal{C} \\ &- 2\alpha\beta\delta_1^2\nu\mathcal{C} - \beta\delta_1\mu^2\nu\mathcal{C} + \beta\delta_1\nu\mathcal{C} + \frac{\alpha\beta\mu^2\nu\mathcal{C}}{2} - \frac{\alpha\beta\nu\mathcal{C}}{2} \\ &+ 4\beta^2\delta_1^2\nu^2 + 4\alpha\beta^2\delta_1\nu^2 + \beta^2\mu^2\nu^2 + \alpha^2\beta^2\nu^2 - \beta^2\nu^2 \\ &+ \frac{\mu^4}{16} + \frac{\delta_1^2\mu^2}{2} - \frac{\mu^2}{8} + \delta_1^4 - \frac{\delta_1^2}{2} + \frac{1}{16} \end{aligned} \tag{4.26}$$

Note that p, q, r, and s all depend on λ appearing in exponential form, so eq. (4.22) is not a polynomial equation. In the previous chapter the Routh-Hurwitz criterion [11] was used to determine the stable regions of the characteristic polynomial, but since eq. (4.22) is a transcendental equation a different technique will have to be used here.

A necessary condition for stability is for the real part of all the eigenvalues λ_i to be nonpositive, and the transition curves between stable and unstable regions in parameter space occur when the real part of λ_i is exactly zero. The approach we'll take to find the transition curves is to set $\lambda = i\omega$; the case when $\omega = 0$ corresponds to a saddle node bifurcation, and all nonzero values of ω correspond to a possible Hopf bifurcation in the nonlinear system.

Substituting $\lambda = i\omega$ in (4.22) turns it into a complex equation, and to solve it we set the real and imaginary parts equal to zero:

$$\begin{aligned} 0 &= 4\beta^2\mu\omega\sin(2\epsilon\omega T) - 4\beta^2\omega^2\cos(2\epsilon\omega T) + 4\beta^2\delta_1^2\cos(2\epsilon\omega T) + 4\alpha\beta^2\delta_1\cos(2\epsilon\omega T) \\ &+ \beta^2\mu^2\cos(2\epsilon\omega T) + \alpha^2\beta^2\cos(2\epsilon\omega T) - \beta^2\cos(2\epsilon\omega T) - 4\beta\omega^3\mathcal{S}\sin(\epsilon\omega T) \end{aligned}$$

$$
\begin{aligned}
&+ \quad 4\beta\delta_1^2\omega\mathcal{S}\sin(\epsilon\omega T) + 4\alpha\beta\delta_1\omega\mathcal{S}\sin(\epsilon\omega T) + 3\beta\mu^2\omega\mathcal{S}\sin(\epsilon\omega T) - \beta\omega\mathcal{S}\sin(\epsilon\omega T) \\
&- \quad 4\beta\mu\delta_1\omega\mathcal{C}\sin(\epsilon\omega T) + 2\alpha\beta\mu\omega\mathcal{C}\sin(\epsilon\omega T) - 6\beta\mu\omega^2\mathcal{S}\cos(\epsilon\omega T) + 2\beta\mu\delta_1^2\mathcal{S}\cos(\epsilon\omega T) \\
&+ \quad 2\alpha\beta\mu\delta_1\mathcal{S}\cos(\epsilon\omega T) + \frac{\beta\mu^3\mathcal{S}\cos(\epsilon\omega T)}{2} - \frac{\beta\mu\mathcal{S}\cos(\epsilon\omega T)}{2} + 4\beta\delta_1\omega^2\mathcal{C}\cos(\epsilon\omega T) \\
&- \quad 2\alpha\beta\omega^2\mathcal{C}\cos(\epsilon\omega T) - 4\beta\delta_1^3\mathcal{C}\cos(\epsilon\omega T) - 2\alpha\beta\delta_1^2\mathcal{C}\cos(\epsilon\omega T) - \beta\mu^2\delta_1\mathcal{C}\cos(\epsilon\omega T) \\
&+ \quad \beta\delta_1\mathcal{C}\cos(\epsilon\omega T) + \frac{\alpha\beta\mu^2\mathcal{C}\cos(\epsilon\omega T)}{2} - \frac{\alpha\beta\mathcal{C}\cos(\epsilon\omega T)}{2} \\
&+ \quad \omega^4 - 2\delta_1^2\omega^2 - \frac{3\mu^2\omega^2}{2} + \frac{\omega^2}{2} + \delta_1^4 + \frac{\mu^2\delta_1^2}{2} - \frac{\delta_1^2}{2} + \frac{\mu^4}{16} - \frac{\mu^2}{8} + \frac{1}{16} \qquad (4.27)
\end{aligned}
$$

$$
\begin{aligned}
0 \quad = \quad & 4\beta^2\omega^2\sin(2\epsilon\omega T) - 4\beta^2\delta_1^2\sin(2\epsilon\omega T) - 4\alpha\beta^2\delta_1\sin(2\epsilon\omega T) - \beta^2\mu^2\sin(2\epsilon\omega T) \\
&- \quad \alpha^2\beta^2\sin(2\epsilon\omega T) + \beta^2\sin(2\epsilon\omega T) + 4\beta^2\mu\omega\cos(2\epsilon\omega T) + 6\beta\mu\omega^2\mathcal{S}\sin(\epsilon\omega T) \\
&- \quad 2\beta\mu\delta_1^2\mathcal{S}\sin(\epsilon\omega T) - 2\alpha\beta\mu\delta_1\mathcal{S}\sin(\epsilon\omega T) - \frac{\beta\mu^3\mathcal{S}\sin(\epsilon\omega T)}{2} + \frac{\beta\mu\mathcal{S}\sin(\epsilon\omega T)}{2} \\
&- \quad 4\beta\delta_1\omega^2\mathcal{C}\sin(\epsilon\omega T) + 2\alpha\beta\omega^2\mathcal{C}\sin(\epsilon\omega T) + 4\beta\delta_1^3\mathcal{C}\sin(\epsilon\omega T) + 2\alpha\beta\delta_1^2\mathcal{C}\sin(\epsilon\omega T) \\
&+ \quad \beta\mu^2\delta_1\mathcal{C}\sin(\epsilon\omega T) - \beta\delta_1\mathcal{C}\sin(\epsilon\omega T) - \frac{\alpha\beta\mu^2\mathcal{C}\sin(\epsilon\omega T)}{2} + \frac{\alpha\beta\mathcal{C}\sin(\epsilon\omega T)}{2} \\
&- \quad 4\beta\omega^3\mathcal{S}\cos(\epsilon\omega T) + 4\beta\delta_1^2\omega\mathcal{S}\cos(\epsilon\omega T) + 4\alpha\beta\delta_1\omega\mathcal{S}\cos(\epsilon\omega T) + 3\beta\mu^2\omega\mathcal{S}\cos(\epsilon\omega T) \\
&- \quad \beta\omega\mathcal{S}\cos(\epsilon\omega T) - 4\beta\mu\delta_1\omega\mathcal{C}\cos(\epsilon\omega T) + 2\alpha\beta\mu\omega\mathcal{C}\cos(\epsilon\omega T) \\
&- \quad 2\mu\omega^3 + 2\mu\delta_1^2\omega + \frac{\mu^3\omega}{2} - \frac{\mu\omega}{2} \qquad (4.28)
\end{aligned}
$$

These equations are very messy, and it is not clear if a closed form solution $T(\delta_1, \alpha, \beta, \mu, \epsilon)$ can be found by eliminating ω. To simplify matters, we will start by setting $\epsilon = 0$ in eqs. (4.27), (4.28), which is equivalent to approximating the delay terms in the slow flow as nondelay terms.

4.3.1 The Non-Delayed Case

Setting $\epsilon = 0$ in eqs. (4.27), (4.28) yields:

$$
0 \quad = \quad -4\beta^2\omega^2 + 4\beta^2\delta_1^2 + 4\alpha\beta^2\delta_1 + \beta^2\mu^2 + \alpha^2\beta^2 - \beta^2 - 6\beta\mu\omega^2\mathcal{S} + 2\beta\mu\delta_1^2\mathcal{S}
$$

$$
\begin{aligned}
&+ \quad 2\alpha\beta\mu\delta_1\mathcal{S} + \frac{\beta\mu^3\mathcal{S}}{2} - \frac{\beta\mu\mathcal{S}}{2} + 4\beta\delta_1\omega^2 C - 2\alpha\beta\omega^2 C - 4\beta\delta_1^3 C - 2\alpha\beta\delta_1^2 C \\
&- \quad \beta\mu^2\delta_1 C + \beta\delta_1 C + \frac{\alpha\beta\mu^2 C}{2} - \frac{\alpha\beta C}{2} + \omega^4 - 2\delta_1^2\omega^2 - \frac{3\mu^2\omega^2}{2} + \frac{\omega^2}{2} \\
&+ \quad \delta_1^4 + \frac{\mu^2\delta_1^2}{2} - \frac{\delta_1^2}{2} + \frac{\mu^4}{16} - \frac{\mu^2}{8} + \frac{1}{16} \qquad (4.29) \\
0 \quad &= \quad 4\beta^2\mu\omega - 4\beta\delta_1\omega^2 C - 4\beta\omega^3\mathcal{S} + 4\beta\delta_1^2\omega\mathcal{S} + 4\alpha\beta\delta_1\omega\mathcal{S} + 3\beta\mu^2\omega\mathcal{S} - \beta\omega\mathcal{S} \\
&- \quad 4\beta\mu\delta_1\omega C + 2\alpha\beta\mu\omega C - 2\mu\omega^3 + 2\mu\delta_1^2\omega + \frac{\mu^3\omega}{2} - \frac{\mu\omega}{2} \qquad (4.30)
\end{aligned}
$$

This system is simple enough to have a closed form solution. We start by solving eq. (4.30) for ω, resulting in the trivial solution:

$$\omega = 0$$

And the nontrivial solution:

$$\omega^2 = \frac{\left(8\beta\delta_1^2 + 8\alpha\beta\delta_1 + 6\beta\mu^2 - 2\beta\right)\mathcal{S} + \left(4\alpha\beta\mu - 8\beta\mu\delta_1\right)C + 4\mu\delta_1^2 + \mu^3 + \left(8\beta^2 - 1\right)\mu}{8\beta\mathcal{S} + 4\mu} \qquad (4.31)$$

The saddle node transition curves are obtained by substituting $\omega = 0$ in eq. (4.29):

$$
\begin{aligned}
0 \quad &= \quad \left(32\beta\mu\delta_1^2 + 32\alpha\beta\mu\delta_1 + 8\beta\mu^3 - 8\beta\mu\right)\mathcal{S} \\
&+ \quad \left(16\beta\delta_1 - 64\beta\delta_1^3 - 32\alpha\beta\delta_1^2 - 16\beta\mu^2\delta_1 + 8\alpha\beta\mu^2 - 8\alpha\beta\right)C \\
&+ \quad 16\delta_1^4 + 8\mu^2\delta_1^2 + 64\beta^2\delta_1^2 - 8\delta_1^2 + 64\alpha\beta^2\delta_1 \\
&+ \quad \mu^4 + 16\beta^2\mu^2 - 2\mu^2 + 16\alpha^2\beta^2 - 16\beta^2 + 1 \qquad (4.32)
\end{aligned}
$$

The Hopf transition curves are obtained by substituting (4.31) in eq. (4.29):

$$
\begin{aligned}
0 \quad &= \quad 128\alpha\beta^3\mu\delta_1\mathcal{S}^3 + 64\beta^3\mu^3\mathcal{S}^3 - 16\alpha^2\beta^3\mu\mathcal{S}^3 - 16\beta^3\mu\mathcal{S}^3 - 128\beta^3\mu^2\delta_1 C\mathcal{S}^2 \\
&+ \quad 32\alpha^2\beta^3\delta_1 C\mathcal{S}^2 + 64\alpha\beta^3\mu^2 C\mathcal{S}^2 + 64\beta^2\mu^2\delta_1^2\mathcal{S}^2 - 16\alpha^2\beta^2\delta_1^2\mathcal{S}^2 + 32\alpha\beta^2\mu^2\delta_1\mathcal{S}^2
\end{aligned}
$$

$$
\begin{aligned}
&+ \quad 48\beta^2\mu^4\mathcal{S}^2 + 128\beta^4\mu^2\mathcal{S}^2 - 4\alpha^2\beta^2\mu^2\mathcal{S}^2 - 20\beta^2\mu^2\mathcal{S}^2 - 16\alpha^2\beta^4\mathcal{S}^2 + 64\alpha\beta^2\mu\delta_1^2 C\mathcal{S} \\
&- \quad 64\beta^2\mu^3\delta_1 C\mathcal{S} - 128\beta^4\mu\delta_1 C\mathcal{S} + 32\alpha\beta^2\mu^3 C\mathcal{S} + 64\alpha\beta^4\mu C\mathcal{S} + 32\beta\mu^3\delta_1^2\mathcal{S} \\
&+ \quad 64\beta^3\mu\delta_1^2\mathcal{S} - 128\alpha\beta^3\mu\delta_1\mathcal{S} + 12\beta\mu^5\mathcal{S} + 64\beta^3\mu^3\mathcal{S} - 8\beta\mu^3\mathcal{S} + 64\beta^5\mu\mathcal{S} \\
&+ \quad 16\alpha\beta\mu^2\delta_1^2 C - 8\beta\mu^4\delta_1 C - 32\beta^3\mu^2\delta_1 C + 4\alpha\beta\mu^4 C + 16\alpha\beta^3\mu^2 C + 4\mu^4\delta_1^2 \\
&+ \quad 16\beta^2\mu^2\delta_1^2 - 32\alpha\beta^2\mu^2\delta_1 + \mu^6 + 8\beta^2\mu^4 - \mu^4 + 16\beta^4\mu^2
\end{aligned} \tag{4.33}
$$

Figure 4.1 shows both the saddle node bifurcation curves and the Hopf bifurcation curves for the non-delayed system, as well as the stable regions. Stable regions are determined by selecting a representative point from each disjoint region and testing that point for stability.

Figure 4.2 compares the transition curves calculated using the Routh-Hurwitz criterion in Chapter 3 with the technique used in this chapter. The stable regions for both techniques are identical, although the Routh-Hurwitz criterion produces additional transition curves which, although necessary for stability, are not sufficient, which is why they do not arise in both methods.

We now return to eqs. (4.27), (4.28) and employ a perturbation approach to calculate the Hopf bifurcation.

4.3.2 The Delayed Case

Since we now have a solution when $\epsilon = 0$, the next reasonable course of action would be to look for a series solution in ϵ with our result being the zeroth order solution. Unfortunately, the result when $\epsilon = 0$ is still too complicated to be written explicitly in a closed form solution. In order to determine the effect of ϵ on the system, we also need to perturb off of α and μ, resulting in a series

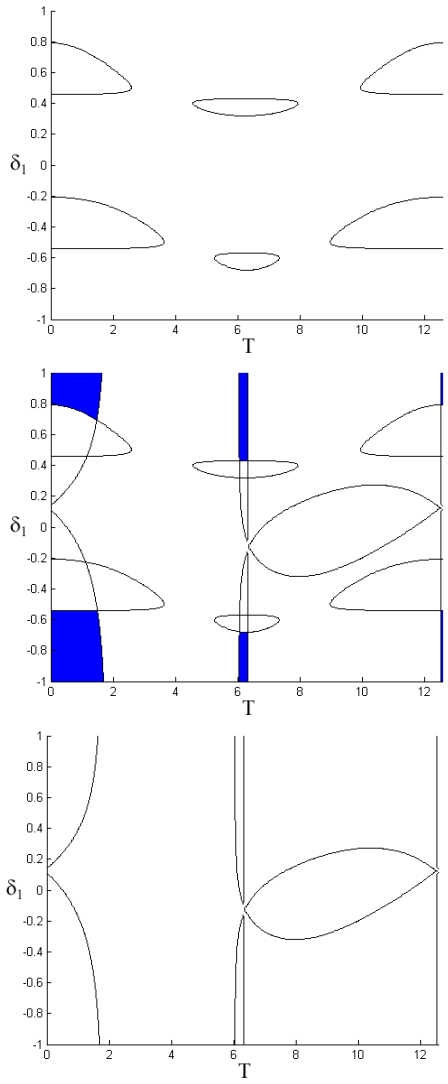

Figure 4.1: Plots of different transition curves for $\alpha = 0.1$, $\beta = 0.125$, and $\mu = 0.01$. Saddle node bifurcations are on the left, Hopf bifurcations are on the right, and the middle shows both.

expansion in three variables.

Fortunately, the saddle node bifurcations are the same for both the delayed and non-delayed systems, since setting $\lambda = i\omega = 0$ is equivalent to replacing the delay terms with nondelay terms, so we do not need to investigate the case when $\omega = 0$ as this solution is already known exactly.

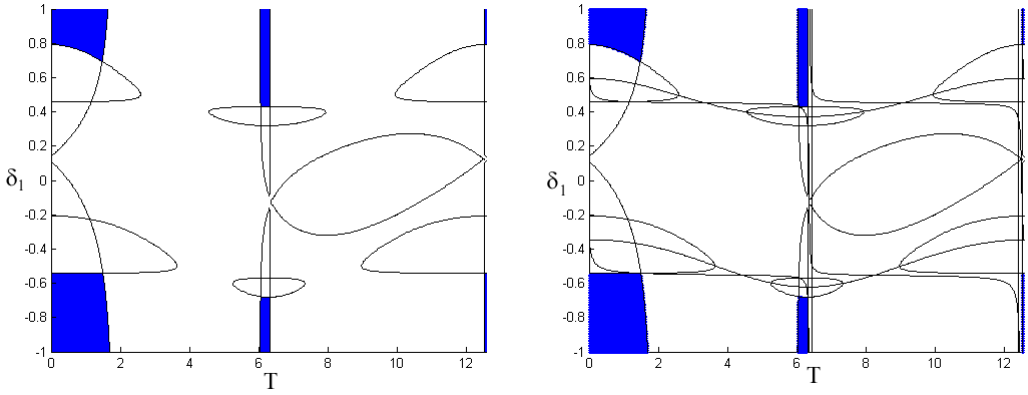

Figure 4.2: Comparison of the transition curves and stable regions calculated from setting $\lambda = i\omega$ (left) with the Routh-Hurwitz criterion (right) for the parameter values of $\alpha = 0.1$, $\beta = 0.125$, $\mu = 0.01$.

We begin by expanding T and ω in the following series:

$$\begin{aligned} T &= T_{000} + T_{100}\alpha + T_{010}\epsilon + T_{001}\mu + T_{200}\alpha^2 + T_{110}\alpha\epsilon \\ &+ T_{101}\alpha\mu + T_{020}\epsilon^2 + T_{011}\epsilon\mu + T_{002}\mu^2 + \cdots \end{aligned} \tag{4.34}$$

$$\begin{aligned} \omega &= \omega_{000} + \omega_{100}\alpha + \omega_{010}\epsilon + \omega_{001}\mu + \omega_{200}\alpha^2 + \omega_{110}\alpha\epsilon \\ &+ \omega_{101}\alpha\mu + \omega_{020}\epsilon^2 + \omega_{011}\epsilon\mu + \omega_{002}\mu^2 + \cdots \end{aligned} \tag{4.35}$$

We first calculate the zeroth order terms T_{000} and ω_{000} and use those results to calculate higher order terms.

Substituting (4.34), (4.35) into eqs. (4.27), (4.28) and setting $\alpha = 0$, $\epsilon = 0$, and $\mu = 0$, eqs. (4.27), (4.28) become:

$$0 = \frac{\left(4\omega_{000}^2 - 4\delta_1^2 + 1\right)\left(16\beta\delta_1 \cos\left(\frac{T_{000}}{2}\right) + 4\omega_{000}^2 - 4\delta_1^2 - 16\beta^2 + 1\right)}{16} \tag{4.36}$$

$$0 = -\beta\omega_{000}\left(4\omega_{000}^2 - 4\delta_1^2 + 1\right)\sin\left(\frac{T_{000}}{2}\right) \tag{4.37}$$

Looking at eq. (4.37), we see there are three distinct cases to examine: $\omega_{000} =$

0; $4\omega_{000}^2 - 4\delta_1^2 + 1 = 0$; and $\sin\left(\frac{T_{000}}{2}\right) = 0$. As we are not interested in the case when $\omega = 0$, we will only focus on the second and third cases.

In the second case when $4\omega_{000}^2 - 4\delta_1^2 + 1 = 0$, eq. (4.36) is also identically zero. Thus, this single condition satisfies both eq. (4.36) and eq. (4.37). In this case, we get $\omega_{000} = \sqrt{\delta_1^2 - \frac{1}{4}}$, which undergoes a Hopf bifurcation when $|\delta_1| > 1/2$.

In the third case when $\sin\left(\frac{T_{000}}{2}\right) = 0$, the condition is satisfied when $T_{000} = 2n\pi$ for integer values of n. In this paper we will examine the smallest nonzero delay at which a Hopf bifurcation occurs, which is when $T_{000} = 2\pi$.

Substituting $T_{000} = 2\pi$ into (4.36) yields the expression:

$$-16\beta\delta_1 + 4\omega_{000}^2 - 4\delta_1^2 - 16\beta^2 + 1 = 0$$

Solving for ω_{000} gives us the solution:

$$\omega_{000} = \frac{\sqrt{4\delta_1^2 + 16\beta\delta_1 + 16\beta^2 - 1}}{2}$$

Since $\omega > 0$ for a Hopf bifurcation, the radicand must be positive. The radicand is positive for $\delta_1 < -2\beta - 1/2$ and $\delta_1 > -2\beta + 1/2$, which fully determines the Hopf bifurcation for the case of $T_{000} = 2\pi$.

This means that the Hopf curve represents a necessary condition for a Hopf bifurcation, but not a sufficient one. The points where the Hopf curve intersect the saddle node curves divide the Hopf curve into disjoint regions; the additional conditions $\delta_1 < -2\beta - 1/2$ and $\delta_1 > -2\beta + 1/2$ are used to determine which of those disjoint regions represent actual Hopf bifurcations.

The third case is the solution we will focus on for the series solution; we will

pick $T_{000} = 2\pi$ and $\omega_{000} = \sqrt{4\delta_1^2 + 16\beta\delta_1 + 16\beta^2 - 1}/2$ as our zeroth order solutions in the perturbation method.

By substituting the zeroth order solutions back into eqs. (4.27), (4.28), we are then able to solve for higher order terms. At each step in this process, ω_{ijk} and T_{ijk} are solved simultaneously, just as ω_{000} and T_{000} were in the zeroth order case. The final result for (4.34), (4.35) is:

$$T = 2\pi + \frac{\mu}{2\beta} - 4\pi(\delta_1 + 2\beta)\epsilon + 2\pi\alpha\epsilon - \frac{\delta_1 + 2\beta}{\beta}\epsilon\mu + 8\pi(\delta_1 + 2\beta)^2\epsilon^2 + \cdots \tag{4.38}$$

$$\begin{aligned}\omega &= \omega_{000} - \frac{1}{2\omega_{000}}(\delta_1 + 2\beta)\alpha - \frac{1}{32\beta\omega_{000}^3}\left(4\delta_1^3 + 24\beta\delta_1^2 + 48\beta^2\delta_1 - \delta_1 + 32\beta^3 - \beta\right)\alpha^2 \\ &- \frac{1}{\omega_{000}}\left(\pi^2\beta\delta_1\right)\epsilon^2 + \frac{\pi}{4\omega_{000}}\epsilon\mu - \frac{1}{16\beta\omega_{000}}(\delta_1 + 2\beta)\mu^2 + \cdots\end{aligned} \tag{4.39}$$

Figure 4.4 shows eq. (4.38) and eq. (4.32).

Since we are mostly concerned with the area around $T = 2\pi$, the graphs shown here will zoom in on that region. A blowup of Figure 4.1 is shown in Figure 4.3 for reference.

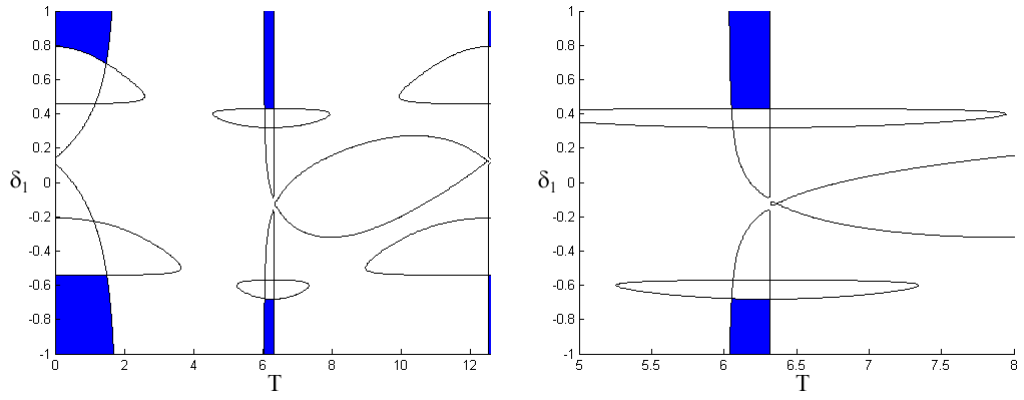

Figure 4.3: A close-up of Figure 4.1 (left) is provided on the right.

Figure 4.5 shows family curves of eq. (4.38) in the $\delta_1 - T$ plane for various values of α, β, ϵ and μ.

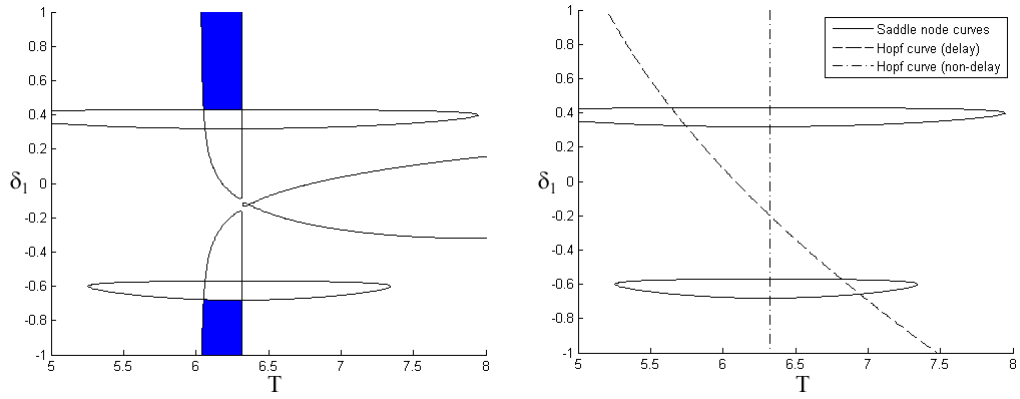

Figure 4.4: Comparison of Figure 4.3 (left) with the series solutions for the Hopf curves, both delayed and non-delayed, and the saddle node bifurcation curves (right).

4.4 Numerical Results

The numerical computations use DDE23 in MATLAB [6] to numerically integrate the linearized slow flow (4.17), (4.18), (4.19), (4.20).

These numerical results will be compared to the analytic results presented in the previous section. We note that the analytic results are approximate due to the perturbation method, which truncates the solution, neglecting higher order terms; in this way both the numerical and the analytic approaches are approximate. Additionally, the slow flow only captures the behavior of the system on the slow time scale, and thus ignores some of the structure of the original system.

We find much better agreement when comparing the analytic results to the numerical integration of the slow flow instead of the numerical integration of the original system, and this stems from the fact that the slow flow is itself only an approximation. Figure 4.6 compares numerical integration of the original system with numerical integration of the slow flow.

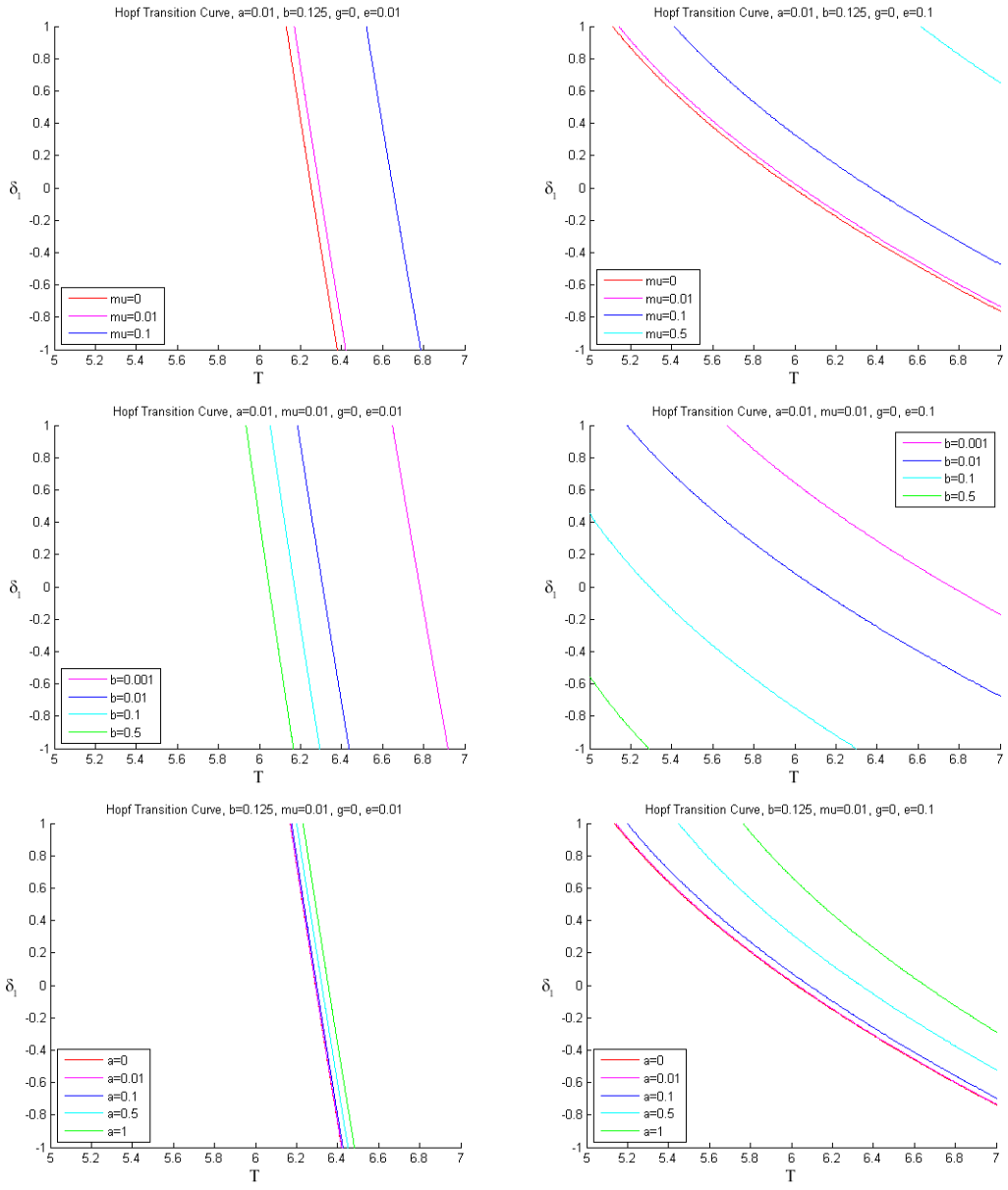

Figure 4.5: Family of Hopf transition curves around $T = 2\pi$. The left column has $\epsilon = 0.01$ and the right column has $\epsilon = 0.1$. The top row varies μ, the middle row varies β, and the bottom row varies α.

The code we used determines stability of the origin by taking the initial condition as a point close to the origin and checking if the amplitude grows without bound. Since nonlinear terms will trap unstable trajectories in a limit cycle of finite amplitude, the techniques outlined here only work with the linearized

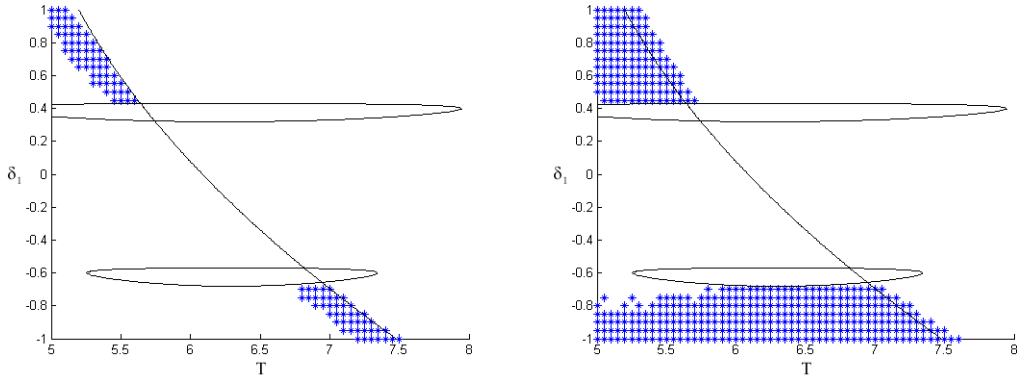

Figure 4.6: Comparison of the results of numerical integration of the slow flow (left) versus the results of numerical integration of the original system (right). The asterisks are stable points and the curves are the saddle node and Hopf transition curves.

system.

We utilized a combination of two techniques to accomplish this goal: first, we select an upper bound on amplitude size and quit out of integration if that amplitude is reached; second, for all other cases we check if the maximum amplitude over the entire time interval is equivalent to the maximum amplitude over a subsection of the time interval. This latter method helps capture edge cases that the former doesn't catch.

In all computations we used $\alpha = 0.1, \beta = 0.125$ and $\mu = 0.01$.

In Figure 4.7 we see the effect of including delay purely from the standpoint of numerical integration. The right graph in the figure also compares the analytic results to the results of numerical integration.

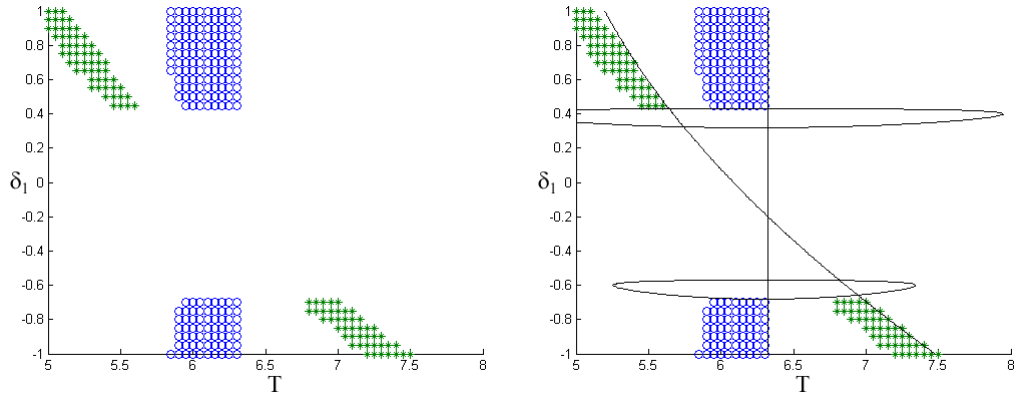

Figure 4.7: Comparison of numerical integration of the slow flow with delay terms (asterisks) and without delay terms (circles). The transition curves are included for the graph on the right.

4.5 Conclusion

In this chapter, we investigated the dynamics of two coupled Mathieu equations with delay. In particular we analyzed the stability of the origin and the effect of delay and damping on stability. We used the method of two variable expansion to calculate a characteristic equation of the system's slow flow, and used power series to analyze the Hopf bifurcations around $T = 2\pi$; these results were then compared with numerical integration.

The numerical results of the slow flow closely matched the analytical results for small values of ϵ, α and μ. Furthermore, within the range of parameter values for which agreement held, we found significant variation in the Hopf bifurcation transition curve. These results demonstrate that including delay terms in the slow flow can be very important when approximating numerical results.

To measure the significance of replacing delay terms by nondelay terms, we calculate the error between the numerical integration of T and the series solution, for both the entire series and just the zeroth order terms. The percent error

is calculated as follows:

$$\text{error} = \frac{|T_{num} - T_{series}|}{T_{num}} \times 100\%$$

For fixed values of δ_1 between -1 and 1, different values of T_{num} and T_{series} are obtained. The table below shows the average and maximum values of the error in this range.

	Zeroth ($\epsilon = 0$)	Full ($\epsilon = 0.1$)
Average	15.04%	0.60%
Maximum	19.34%	1.88%

Even looking at the maximum possible error, including delay terms results in a more accurate solution by a factor of 10. When looking at the average, the accuracy is even better. This demonstrates what is lost by omitting the delay terms in the slow flow.

CHAPTER 5

NONLINEARITY AND ONE WAY COUPLING

5.1 Introduction

The fourth and last variation on eqs. (1.1), (1.2) generalizes the previous models to include any arbitrary number of bunches. To help make things simpler, we completely omit the delay terms from the model by assuming that the strength of resistive wall coupling is negligible compared to the strength of electron cloud coupling.

The model for this chapter is:

$$\ddot{x}_1 + (\delta + \epsilon \cos t)x_1 + \epsilon\gamma x_1^3 + \epsilon\mu\dot{x}_1 = 0 \tag{5.1}$$

$$\ddot{x}_i + (\delta + \epsilon \cos t)x_i + \epsilon\gamma x_i^3 + \epsilon\mu\dot{x}_i = \epsilon\alpha x_{i-1} \quad , \quad 2 \leq \mathrm{i} \leq n \tag{5.2}$$

Because the α term only couples a bunch with the bunch in front of it, this model emphasizes the effect of one-way coupling. We will also focus more on the effect of the nonlinear term in this model by examining the size of possible limit cycles for each bunch.

As in the previous two chapters, we start the analysis by applying a perturbation technique called two variable expansion.

5.2 Two Variable Expansion

We use the two variable expansion method [4], [10] to study the dynamics of eqs. (5.1), (5.2). We set

$$\xi(t) = t, \quad \eta(t) = \epsilon t$$

where ξ is the time t and η is the slow time.

Since the x_i terms are functions of ξ and η, the derivative with respect to time t is expressed through the chain rule:

$$\dot{x}_i = x_{i_\xi} + \epsilon x_{i_\eta}, \quad 1 \le i \le n$$

Similarly, for the second derivative we obtain:

$$\ddot{x}_i = x_{i_{\xi\xi}} + 2\epsilon x_{i_{\xi\eta}} + \epsilon^2 x_{i_{\eta\eta}}, \quad 1 \le i \le n$$

We will only perturb up to $O(\epsilon)$, and so we will ignore the ϵ^2 terms.

We then expand the x_i terms in a power series in ϵ:

$$x_i(\xi, \eta) = x_{i_0}(\xi, \eta) + \epsilon x_{i_1}(\xi, \eta) + O(\epsilon^2), \quad 1 \le i \le n \tag{5.3}$$

In addition, we detune off of the 2:1 subharmonic resonance by setting:

$$\delta = \frac{1}{4} + \epsilon\delta_1 + O(\epsilon^2) \tag{5.4}$$

Substituting (5.3), (5.4) into (5.1), (5.2) and collecting terms in ϵ, we arrive at the following equations:

$$x_{i_{0,\xi\xi}} + \frac{1}{4}x_{i_0} = 0, \quad 1 \le i \le n \tag{5.5}$$

$$x_{1_{1,\xi\xi}} + \frac{1}{4}x_{1_1} = -2x_{i_{0,\xi\eta}} - \gamma x_{i_0}^3 - \mu x_{i_{0,\xi}} - \delta_1 x_{i_0} - x_{i_0}\cos\xi \tag{5.6}$$

$$x_{i_{1,\xi\xi}} + \frac{1}{4}x_{i_1} = -2x_{i_{0,\xi\eta}} - \gamma x_{i_0}^3 - \mu x_{i_{0,\xi}} - \delta_1 x_{i_0} - x_{i_0}\cos\xi - \alpha x_{i-1_0}, \quad 2 \le i \le n \tag{5.7}$$

The solution to (5.5) is simply:

$$x_{i_0} = A_i(\eta)\cos\left(\frac{\xi}{2}\right) + B_i(\eta)\sin\left(\frac{\xi}{2}\right), \quad 1 \le i \le n \tag{5.8}$$

We then substitute (5.8) into (5.6), (5.7). Using trigonometric identities, these equations can be written in terms of $\cos\frac{\xi}{2}$ and $\sin\frac{\xi}{2}$. We set the coefficients of such terms equal to zero in order to remove the secular terms which cause resonance. This results in $2n$ equations in $2n$ unknowns:

$$A_1' = -\frac{B_1}{2} + \delta_1 B_1 - \frac{\mu A_1}{2} + \frac{3\gamma}{4}B_1(A_1^2 + B_1^2) \tag{5.9}$$

$$B_1' = -\frac{A_1}{2} - \delta_1 A_1 - \frac{\mu B_1}{2} - \frac{3\gamma}{4}A_1(A_1^2 + B_1^2) \tag{5.10}$$

$$\vdots$$

$$A_i' = -\frac{B_i}{2} + \delta_1 B_i - \frac{\mu A_i}{2} + \frac{3\gamma}{4}B_i(A_i^2 + B_i^2) - \alpha B_{i-1} \quad , \quad 2 \le \mathrm{i} \le n \tag{5.11}$$

$$B_i' = -\frac{A_i}{2} - \delta_1 A_i - \frac{\mu B_i}{2} - \frac{3\gamma}{4}A_i(A_i^2 + B_i^2) + \alpha A_{i-1} \quad , \quad 2 \le \mathrm{i} \le n \tag{5.12}$$

These equations are known as the slow flow of the system and represent the envelope of the oscillatory motion of equations (5.1), (5.2). Finding the equilibrium points of the slow flow is analogous to finding simple harmonic motion with constant amplitude in the original system. In doing so we will not only obtain information on the amplitude of these limit cycles, but also information on where Hopf bifurcations occur in parameter space.

5.3 Analytic Results

5.3.1 The First Bunch

The dynamics of the first bunch are given by eqs. (5.9), (5.10).

$$\begin{aligned} A_1' &= -\frac{B_1}{2} + \delta_1 B_1 - \frac{\mu A_1}{2} + \frac{3\gamma}{4} B_1 (A_1^2 + B_1^2) \\ B_1' &= -\frac{A_1}{2} - \delta_1 A_1 - \frac{\mu B_1}{2} - \frac{3\gamma}{4} A_1 (A_1^2 + B_1^2) \end{aligned}$$

As this system is 2-dimensional, the complete dynamics can be expressed in the phase plane $A_1 - B_1$. The Numerical Results section contains various graphs demonstrating the full dynamics of the first bunch, but the rest of this section will focus purely on calculating the equilibrium points of the system.

Setting these equations equal to zero gives us the following equilibrium points:

$$\begin{aligned} (A_1^*, B_1^*) &= (0,0), \\ &= \left(0, \pm\sqrt{\frac{\pm\sqrt{1-\mu^2}(2\delta_1 - 1) - \mu^2 + 1 - 2\delta_1}{3\gamma}}\right), \\ &= \left(\pm\sqrt{\frac{\pm\sqrt{1-\mu^2}(2\delta_1 + 1) + \mu^2 - 1 - 2\delta_1}{3\gamma}}, 0\right) \end{aligned}$$

Here we use the standard notation A_i^*, B_i^* to denote equilibrium points of the variables A_i, B_i.

To simplify matters, we will focus on the special case when $\delta_1 = 0$ and $\mu = 0$. The fixed points in this case are:

$$(A_1^*, B_1^*) = (0,0), \left(0, \pm\sqrt{\frac{2}{3\gamma}}\right), \left(\pm i\sqrt{\frac{2}{3\gamma}}, 0\right) \tag{5.13}$$

Here we note our first major observation: Nontrivial real equilibrium points for A_1 only exist for $\gamma < 0$, and nontrivial real equilibrium points for B_1 only exist for $\gamma > 0$. However, the magnitude of the amplitude is the same in both cases, and the analysis of both cases is identical. Without loss of generality, we will take $\gamma > 0$ and $A_1^* = 0$.

5.3.2 The Second Bunch

The dynamics of the second bunch are given when $i = 2$ in eqs. (5.11), (5.12).

$$A_2' = -\frac{B_2}{2} + \delta_1 B_2 - \frac{\mu A_2}{2} + \frac{3\gamma}{4} B_2(A_2^2 + B_2^2) - \alpha B_1 \tag{5.14}$$

$$B_2' = -\frac{A_2}{2} - \delta_1 A_2 - \frac{\mu B_2}{2} - \frac{3\gamma}{4} A_2(A_2^2 + B_2^2) + \alpha A_1 \tag{5.15}$$

Note that these equations share a similar structure to eqs. (5.9), (5.10) but with additional terms resulting from the one-way coupling. These additional terms mean the dynamics of the second bunch is 4-dimensional instead of 2-dimensional like the first bunch, and we cannot view the dynamics in a phase plane. Our analysis of the second bunch will focus only on the steady state solutions and not on the general dynamics.

Since we are taking $\gamma > 0$, all equilibrium points for the first bunch require $A_1^* = 0$; substituting $A_1^* = 0$ into eqs. (5.14), (5.15) yields:

$$\frac{B_2^*[3\gamma(A_2^{*^2} + B_2^{*^2}) - 2] - 4\alpha B_1^*}{4} = 0 \tag{5.16}$$

$$\frac{A_2^*[3\gamma(A_2^{*^2} + B_2^{*^2}) + 2]}{4} = 0 \tag{5.17}$$

Note that $A_2^{*^2} + B_2^{*^2}$ is a nonnegative value, and is only identically zero in the

trivial solution $(A_2^*, B_2^*) = (0, 0)$. Since we are interested in nontrivial solutions, we require that $A_2^{*^2} + B_2^{*^2}$ be positive.

However, since $\gamma > 0$, the expression $3\gamma(A_2^{*^2} + B_2^{*^2}) + 2$ must be positive. Thus, the only way for (5.17) to equal zero is for $A_2^* = 0$.

Substituting $A_2^* = 0$ into (5.16) yields:

$$\frac{3\gamma}{4}B_2^{*^3} - \frac{1}{2}B_2^* - \alpha B_1^* = 0 \tag{5.18}$$

Since B_1^* is already known to us from eq. (5.13), solving this cubic equation will give us the solution for B_2^*.

Note that this solution is for the steady-state of B_2. The full dynamics of the system is 4-dimensional, involving A_1, B_1, A_2 and B_2, and cannot be expressed in a phase plane.

A graph of the relationship between B_2^* and α can be seen in Figure 5.1.

5.3.3 The Third Bunch

The dynamics of the third bunch are given when $i = 3$ in eqs. (5.11), (5.12).

$$A_3' = -\frac{B_3}{2} + \delta_1 B_3 - \frac{\mu A_3}{2} + \frac{3\gamma}{4}B_3(A_3^2 + B_3^2) - \alpha B_2 \tag{5.19}$$

$$B_3' = -\frac{A_3}{2} - \delta_1 A_3 - \frac{\mu B_3}{2} - \frac{3\gamma}{4}A_3(A_3^2 + B_3^2) + \alpha A_2 \tag{5.20}$$

Note that these equations share the *exact* same structure as eqs. (5.14), (5.15). Just like with the second bunch, the presence of additional terms means the dynamics of the third bunch is 4-dimensional. This means that we can't view

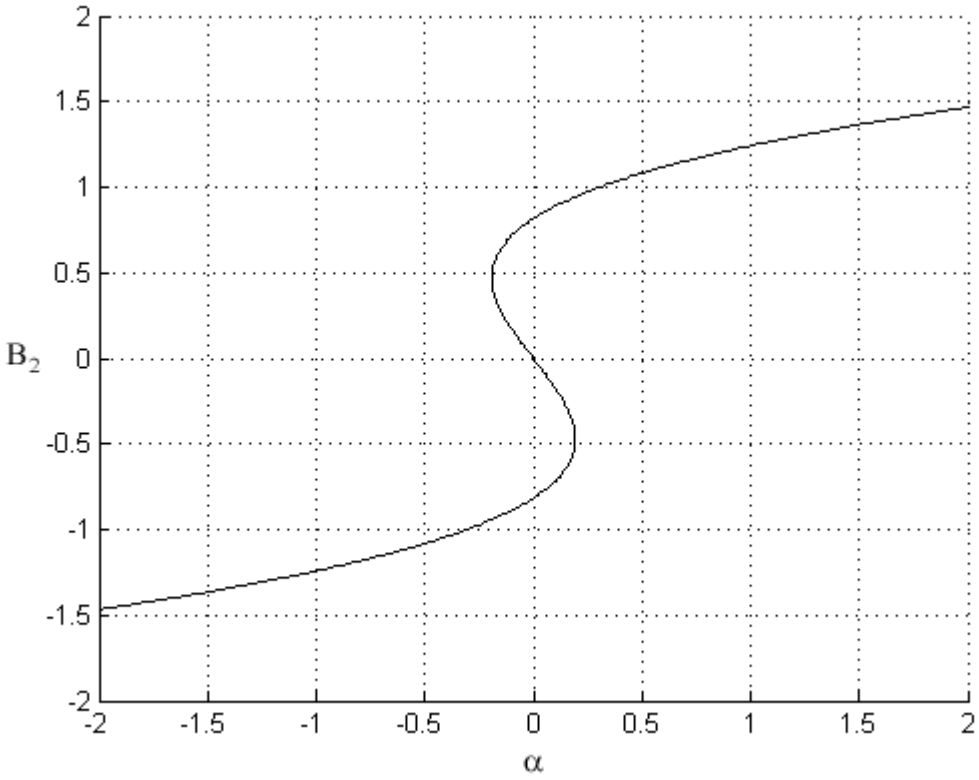

Figure 5.1: Plot of B_2^* as a function of α, for $\gamma = 1$.

the dynamics in a phase plane, and so our analysis of the third bunch will focus only on the steady state solutions and not on the general dynamics.

We know from the analysis of the second bunch that $A_2^* = 0$ is necessary for all steady state solutions of the second bunch; substituting $A_2^* = 0$ into eqs. (5.19), (5.20) yields:

$$\frac{B_3^*[3\gamma(A_3^{*^2} + B_3^{*^2}) - 2] - 4\alpha B_2^*}{4} = 0 \tag{5.21}$$

$$\frac{A_3^*[3\gamma(A_3^{*^2} + B_3^{*^2}) + 2]}{4} = 0 \tag{5.22}$$

Note that $A_3^{*^2} + B_3^{*^2}$ is a nonnegative value, and is only identically zero in the trivial solution $(A_3^*, B_3^*) = (0, 0)$. Since we are interested in nontrivial solutions,

we require that $A_3^{*^2} + B_3^{*^2}$ be positive.

However, since $\gamma > 0$, the expression $3\gamma(A_2^{*^2} + B_2^{*^2}) + 2$ must be positive. Thus, the only way for (5.22) to equal zero is for $A_3^* = 0$.

Substituting $A_3^* = 0$ into (5.21) yields:

$$\frac{3\gamma}{4}B_3^{*^3} - \frac{1}{2}B_3^* - \alpha B_2^* = 0 \tag{5.23}$$

Since B_2^* is already known to us from eq. (5.18), solving this cubic equation will give us the solution for B_3^*.

Given the similarity between eq. (5.23) and eq. (5.18), it is natural to ask if this pattern continues for all later bunches. Indeed, this is the case, and so we will generalize the results found in these past two sections to the n^{th} bunch in the system, where n can be any integer.

5.3.4 The n^{th} Bunch

Due to the nature of one-way coupling, the dynamics of all the bunches except the first one are identical, as can be seen in the results found for the second and third bunches. Thus, we can easily derive a formula for calculating the steady state solution for the n^{th} bunch for any $n > 1$:

$$\frac{3\gamma}{4}B_n^{*^3} - \frac{1}{2}B_n^* - \alpha B_{n-1}^* = 0 \tag{5.24}$$

Unfortunately, calculating B_n^* in practice requires calculating the amplitudes of *all* bunches in front of it, since the recursive relationship cannot be simplified into a formula dependent only on the first bunch. Part of the problem is that

each step requires solving a cubic equation which, although solvable in principle, is a tangled mess. In practice it is much easier to use numerical root solving methods to find the amplitudes for all the bunches.

The other, bigger problem is that cubic equations have three roots; if all three roots are real and distinct, then we have a multi-valued function. Fortunately, this only occurs for a range of α values, and we can easily determine this region through analytic means.

5.3.5 Multi-Valued Regions

Note that in Figure 5.1 there are two points with infinite slope: these are the points that divide the function into multi-valued regions and single valued regions. If we flipped the two axes, then these two points change from having infinite slope to zero slope (see Figure 5.2). Thus, we want to derive $\frac{\mathrm{d}\alpha}{\mathrm{d}B_n^*}$ and find the values of α for which the derivative is equal to zero.

We start by moving the α term in eq. (5.24) to the right hand side and differentiating both sides.

$$\left(\frac{9\gamma}{4}B_n^{*^2} - \frac{1}{2}\right)\mathrm{d}B_n^* = B_{n-1}^*\mathrm{d}\alpha$$

Here B_{n-1}^* is a constant since we're assuming all B_i^* up to $i = n-1$ have already been found.

Solving for $\frac{\mathrm{d}\alpha}{\mathrm{d}B_n^*}$, we obtain:

$$\frac{\mathrm{d}\alpha}{\mathrm{d}B_n^*} = \frac{1}{B_{n-1}^*}\left(\frac{9\gamma}{4}B_n^{*^2} - \frac{1}{2}\right)$$

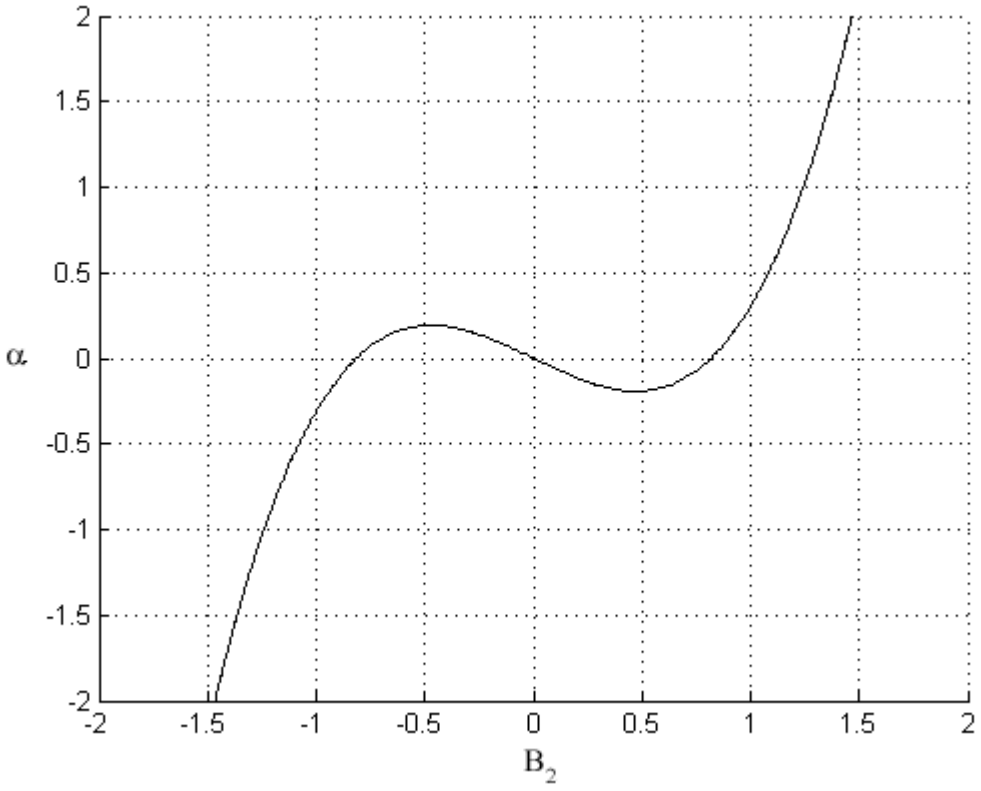

Figure 5.2: Plot of α as a function of B_2^*, for $\gamma = 1$.

We set this equal to zero to find the local extrema:

$$\frac{9\gamma}{4}B_n^{*^2} - \frac{1}{2} = 0 \quad \Rightarrow \quad B_n^* = \pm\sqrt{\frac{2}{9\gamma}}$$

Finally, we substitute this result into eq. (5.24) to find the corresponding α value:

$$B_{n-1}^*\alpha = \left(\frac{3\gamma}{4}\left(\frac{2}{9\gamma}\right) - \frac{1}{2}\right)\left(\pm\sqrt{\frac{2}{9\gamma}}\right) \quad \Rightarrow \quad \alpha = \pm\frac{1}{B_{n-1}^*}\sqrt{\frac{2}{81\gamma}} \tag{5.25}$$

One important feature of this result is that the range of α values for the n^{th} bunch depends on the bunch before it. As an example, for B_2^* the α range depends on $B_1^* = \sqrt{\frac{2}{3\gamma}}$; multiple limit cycles are possible for B_2^* when $\alpha \in [-3^{-3/2}, 3^{-3/2}] \approx (-0.2, 0.2)$.

The significance of this result is that fixing α does *not* guarantee that *all* bunches B_i^* will be either multi-valued or single valued; it is possible to choose α such that B_2^* only has one limit cycle, but B_3^* has three.

A natural question to ask at this point is whether there exist values of α that *do* guarantee single valuedness for all B_i^*. Due to the relationship of eq. (5.25), a uniform bound on α requires a uniform bound on B_i^*, so this question is equivalent to asking if there is a bound on how large B_i^* can become.

5.3.6 Limit as n$\to \infty$

It turns out that the B_i^* are indeed bound by an upper bound, and this can be shown by examining the limit as $n \to \infty$.

In particular, we care about the limit of the amplitude $|B_n^*|$. One way for this limit to exist is if $B^* = B_n^* = B_{n-1}^*$ as $n \to \infty$. In this case, each bunch has the same amplitude as the bunch before it, and each bunch is oscillating in phase with the bunch before it.

By setting $B^* = B_{n-1}^* = B_n^*$ in eq. (5.24), we obtain:

$$B^* \left(\frac{3\gamma}{4} B^{*2} - \frac{1}{2} - \alpha \right) = 0 \tag{5.26}$$

Thus, we find that the possible in-phase limits are:

$$B^* = 0, \ \pm \sqrt{\frac{2(1+2\alpha)}{3\gamma}} \tag{5.27}$$

As long as $\alpha \geq -1/2$, these three limits are distinct; otherwise no in-phase limit cycles are possible.

Another possibility is to examine the case when $B^* = B_n^* = -B_{n-1}^*$ as $n \to \infty$. In this case, each bunch has the same amplitude as the bunch before it, and each bunch is oscillating 180 degrees out of phase with the bunch before it.

By setting $B^* = B_{n-1}^* = -B_n^*$ in eq. (5.24), we obtain:

$$B^* \left(\frac{3\gamma}{4} B^{*^2} - \frac{1}{2} + \alpha \right) = 0 \tag{5.28}$$

Thus, we find that the possible limits are:

$$B^* = 0, \ \pm \sqrt{\frac{2(1-2\alpha)}{3\gamma}} \tag{5.29}$$

As long as $\alpha \leq 1/2$, these three limits are distinct; otherwise no out-of-phase limit cycles are possible.

Therefore, in the limit as $n \to \infty$ there are three possible cases:

- For $\alpha < -1/2$, only out-of-phase limit cycles can exist.
- For $-1/2 < \alpha < 1/2$, both out-of-phase and in-phase limit cycles can exist.
- For $1/2 < \alpha$, only in-phase limit cycles can exist.

Figure 5.3 shows the upper bound for both types of limit cycles.

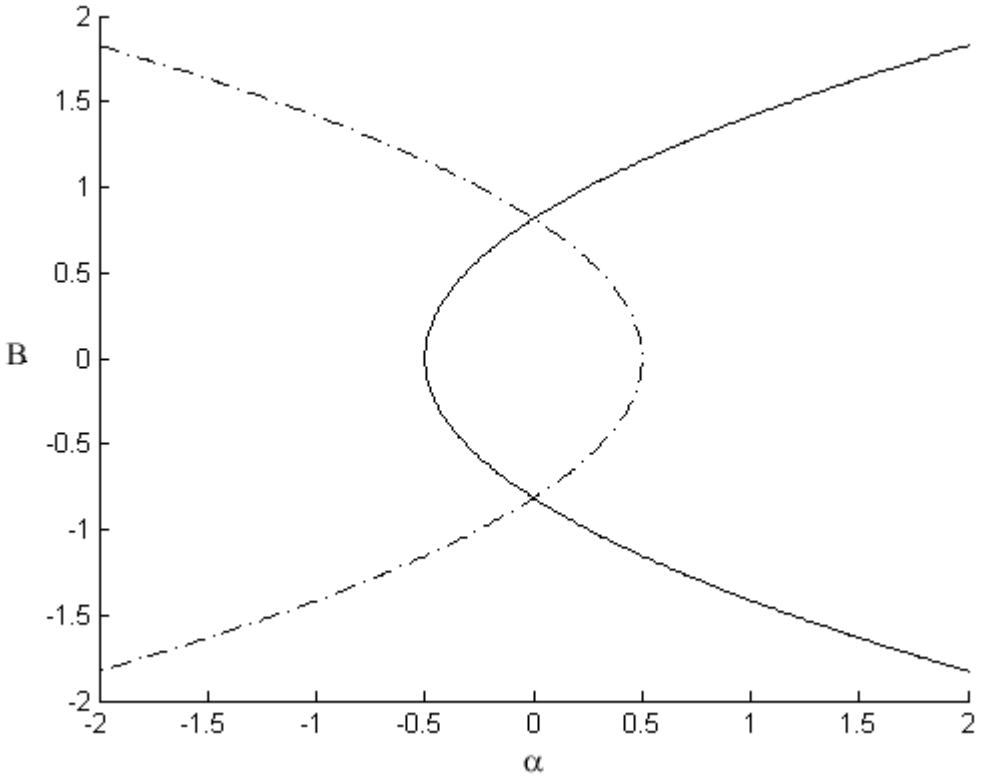

Figure 5.3: Plot of the upper bound on amplitudes for the in-phase limit cycle (solid) and out-of-phase limit cycle (dashed-dot).

5.4 Numerical Results

5.4.1 Phase Plane

To help visualize the dynamics of the first bunch, graphs showing the phase plane for eqs. (5.9), (5.10) are provided below. All phase plane graphs were made using PPLANE [9].

Figure 5.4 compares the cases when $\gamma > 0$ and $\gamma < 0$. Qualitatively the graphs are the same; the only difference is that one has the equilibrium points on the A

axis and the other has the equilibrium points on the B axis.

Figure 5.5 shows the effect of including small values of δ_1 and μ. The inclusion of damping has broken the homoclinic orbit and all orbits are eventually attracted to one of the two stable equilibrium points. Since the two basins of attraction are intertwined, it can be hard in practice to determine which equilibrium point will be reached from a given initial condition.

Figure 5.6 shows the effect of including larger values of δ_1 and μ. The equilibrium points have gone through a pitchfork bifurcation and there is now only one equilibrium point: the origin.

5.4.2 Cobweb Diagram

Since all bunches other than the first bunch are coupled to another bunch, we cannot express their dynamics in a phase plane. Instead, we will show the amplitudes B_1^* through B_n^* in a cobweb diagram for a fixed number n.

Each diagram contains the graphs of eq. (5.24), with B_n^* on the x-axis and B_{n-1}^* on the y-axis, and the line $y = x$. The sequence starts with B_1^* on the x-axis, and proceeds as follows:

- Move vertically to the line $y = x$.
- Move horizontally to the curve given by eq. (5.24) [may be multi-valued].

This process is repeated n times, with each horizontal change determining the next value of B_i^*.

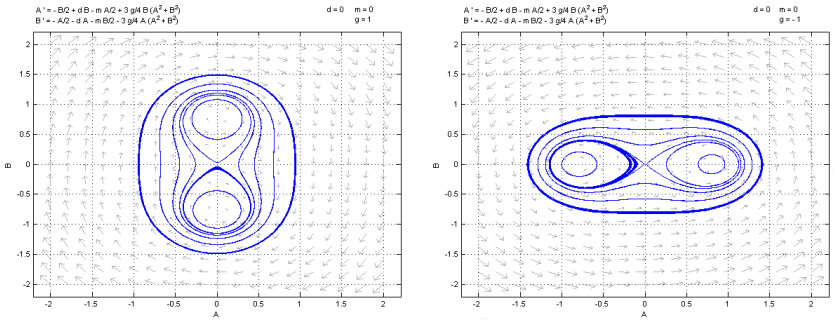

Figure 5.4: Phase plots of the A_1-B_1 dynamics. The left plot shows the dynamics for $\gamma = 1$ and the right plot shows the dynamics for $\gamma = -1$. Both plots have $\alpha = 0$ and $\mu = 0$.

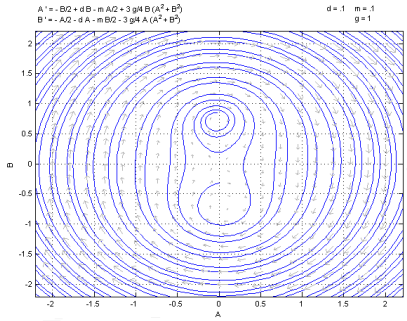

Figure 5.5: Phase plot of the A_1-B_1 dynamics for $\alpha = 0.1$, $\mu = 0.1$ and $\gamma = 1$.

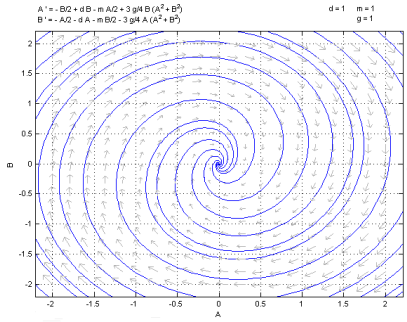

Figure 5.6: Phase plot of the A_1-B_1 dynamics for $\alpha = 1$, $\mu = 1$ and $\gamma = 1$.

For example, Figure 5.7 shows the case when $\alpha > 1/2$. The diagram begins at the point $(0.8, 0)$, representing the value $B_1^* = \sqrt{2/3}$. After moving up to the line $y = x$ at $(0.8, 0.8)$, the process then moves to the right to $(1.1, 0.8)$, where 1.1 represents the next value, B_2^*. After several iterations, the values of B_i^* approach

the point $(1.2, 1.2)$, where 1.2 is the size of the stable limit cycle in this region.

Figure 5.8 shows the case when $\alpha < -1/2$. The diagram begins at the point $(0.8, 0)$, as before. This time, after moving up to the point $(0.8, 0.8)$, the process then moves to the left to $(-1.2, 0.8)$, where -1.2 represents the next value, B_2^*. After several iterations, the values of B_i^* alternate between two values, 1.3 and -1.3, reflecting the out-of-phase nature of the stable limit cycle in this region.

For $-1/2 < \alpha < 1/2$, there are three possible limit cycles. Since the output of eq. (5.24) is multi-valued in this region, there are many different cobweb diagrams for a given starting point B_1^*, with the realized outcome determined by the initial condition in the original system (5.1), (5.2). The code used to generate the diagrams picks one of the three limit cycles at random, as this best represents the unpredictability of knowing the precise initial condition.

Figure 5.9 shows the chaotic nature of this iteration map in the region $-1/2 < \alpha < 1/2$. Since the behavior here is randomized, there is no clear pattern to be discerned here. However, we note that the attractor seems to be a fractal of some kind since there are gaps that are never reached.

5.4.3 Convergence to the Limit

The most important question in this model is determining how long a train of bunches can be before the tail becomes unstable. We have shown that there is a theoretical upper bound to the limit cycle amplitude, but it remains to be seen how quickly the numerical sequence given by eq. (5.24) approaches this limit.

Figure 5.10 shows a sequence of graphs of B_n^* vs α for $2 \leq n \leq 5$ and $\alpha >$

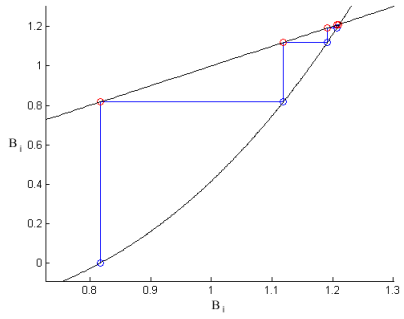

Figure 5.7: Cobweb diagram for $\alpha = 0.6$ and $\gamma = 1$.

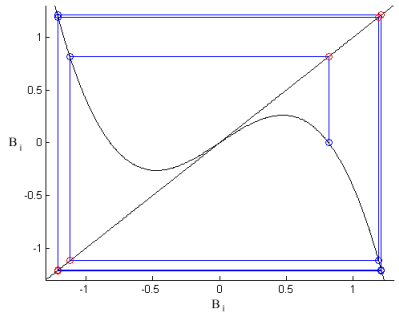

Figure 5.8: Cobweb diagram for $\alpha = -0.6$ and $\gamma = 1$.

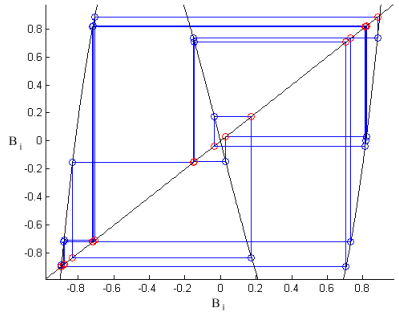

Figure 5.9: Cobweb diagram for $\alpha = 0.1$ and $\gamma = 1$.

0.5, which demonstrates the speed at which this sequence approaches the limit. However, we note that the sequence does not seem to have a constant rate of convergence, and for larger α values it takes longer to converge to the limit.

Figure 5.11 shows the graph of B_5^* vs α for a larger range of α values, including the multi-valued region. While the multi-valued region does not show

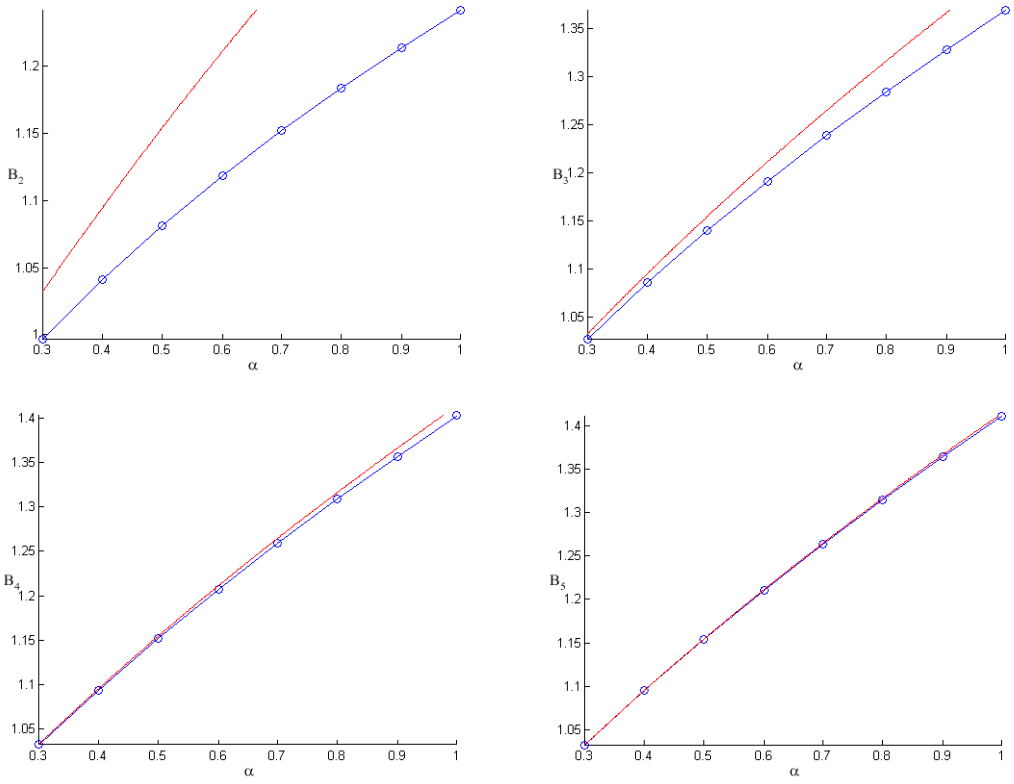

Figure 5.10: Plots of B_n^* vs α for $\alpha > 0.5$ and $\gamma = 1$. The top left graph shows $n = 2$, the top right graph shows $n = 3$, the bottom left graph shows $n = 4$, and the bottom right graph shows $n = 5$.

convergence to either of the limit curves, the values do stay bounded between the maximum values of the two limit curves. Thus, even in this region we can place an upper bound on how large the B_i^* can grow.

Figure 5.12 shows the graph of B_6^* vs α. For $\alpha > 0.5$, this figure is almost identical to Figure 5.11, but for $\alpha < -0.5$ the sign of the curve is now negative instead of positive. This reflects how the limit cycle in this region is out-of-phase, as B_6^* is out of phase with B_5^*. Since the magnitude of the limit curve is the same for both positive and negative branches, the sign of B_n^* is of little concern.

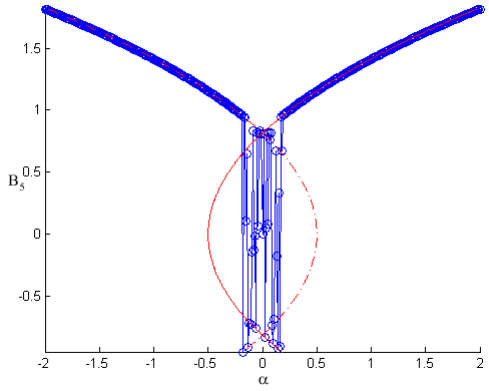

Figure 5.11: Plots of B_5^* vs α for $-2 \leq \alpha \leq 2$ and $\gamma = 1$.

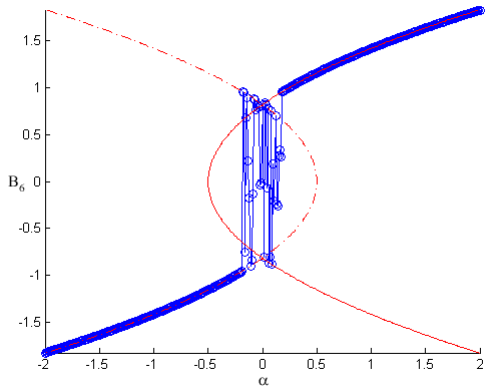

Figure 5.12: Plots of B_6^* vs α for $-2 \leq \alpha \leq 2$ and $\gamma = 1$.

5.5 Conclusion

Our model predicts an upper bound for the amplitudes of bunches in a train. While the dynamics of the system varies depending on the value of α, the upper bound holds for all values of α.

In theory this means that all trajectories are bounded, but in practice there is a physical bound on how large amplitudes can grow before they become unstable. For example, if the theoretical bound on the motion is 100 centimeters, but the radius of the cross-section of the accelerator is only 2 centimeters, then

instability occurs once B_n^* grows larger than 2 centimeters. On the other hand, if the theoretical bound on the motion is 1 centimeter, then instability will never occur, as B_n^* will never grow larger than 2 centimeters.

If it is known that the physical upper bound is smaller than the theoretical upper bound, then it is a simple matter to numerically calculate B_n^* from eq. (5.24) and determine at what point B_n^* exceeds the physical bound. Even in the multi-valued region, taking the worst-case scenario when the amplitude grows the largest at each step will determine the critical n at which instability occurs. Thus, it is possible to know how many bunches to include in a train before instability occurs.

If this model proves accurate, then α can be used to determine the maximum number of bunches in a train. As α contains information for both the per-bunch charge and the per-bunch spacing, adjusting either of these specifications can adjust the value of α, and thus affect the size of the train.

APPENDIX A

A.1 Proof of Structural Instability When $\mu = 0$ and $\alpha \neq 0$

The proof of this phenomenon can be seen by examining the $pqr - r^2 - p^2 s \geq 0$ stability condition when $\mu = 0$ (see eqs. (3.22)-(3.25)):

$$\text{For instability } pqr - r^2 - p^2 s = -16\alpha^2\beta^2\mathcal{S}^2\left(\beta^2 - 2\beta\delta_1 C + \delta_1^2\right) < 0$$

Note that α^2, β^2, and $\mathcal{S}^2$ are all positive, and so $\beta^2 - 2\beta\delta_1 C + \delta_1^2$ needs to be positive for the system to be unstable.

If $C = 0$ (i.e. if $\cos\frac{T}{2} = 0$, i.e. if $T = n\pi$, $n = 1, 3, 5, \cdots$) then $\beta^2 - 2\beta\delta_1 C + \delta_1^2$ is positive. Therefore, by continuity, in order for $\beta^2 - 2\beta\delta_1 C + \delta_1^2$ to become negative it must first pass through zero. But the equation

$$\beta^2 - 2\beta\delta_1 C + \delta_1^2 = 0$$

which is a quadratic on δ_1, cannot have real roots δ_1 since the discriminant is

$$4\beta^2(C^2 - 1) < 0 \text{ if } C^2 \neq 1$$

Thus for a nonzero value of α (and $\mu = 0$) the system is unstable almost everywhere.

The special case $T = n\pi$, $n = 2, 4, 6, \cdots$, gives $C = \cos\frac{T}{2} = \pm 1$, and is excluded from this argument; this case may (and indeed does) correspond to a stable region of measure zero in the $T - \delta_1$ plane.

BIBLIOGRAPHY

[1] Anonymous. Cornell electron storage ring, 2014. http://www.lepp.cornell.edu/Research/CESR/WebHome.html.

[2] J. Guckenheimer and P. Holmes. *Nonlinear Oscillations, Dynamicsl Systems, and Bifurcations of Vector Fields*, volume 42 of *Applied Mathematical Sciences*. Springer, 1983.

[3] C.S. Hsu. On a restricted class of coupled hill's equations and some applications. *Journal of Applied Mechanics*, 1961.

[4] J. Kevorkian and J.D. Cole. *Perturbation Methods in Applied Mathematics*, volume 34 of *Applied Mathematical Sciences*. Springer, 1981.

[5] P.M.M. Mathieu. Le mouvement vibratoire d'une membrane de forme elliptique. Online copy of original text, http://www.math.cornell.edu/ rand/randdocs/classics/Mathieu.pdf.

[6] The MathWorks. MATLAB's reference on dde23. http://www.mathworks.com/help/matlab/ref/dde23.html.

[7] R.E. Meller, 12 2013. Personal communication to author Richard Rand.

[8] T.M. Morrison and R.H. Rand. Resonance in the delayed nonlinear mathieu equation. *Nonlinear Dynamics*, 341-352(doi:10.1007/s11071-006-9162-5), 2007.

[9] J.C. Polking. Ode software for matlab. http://math.rice.edu/ dfield/.

[10] R.H. Rand. Lecture notes in nonlinear vibrations, 2012. http://ecommons.library.cornell.edu/handle/1813/28989.

[11] E.J. Routh. *A treatise on the stability of a given state of motion, particularly steady motion*. Macmillan, 1877.

[12] J.J. Stoker. *Nonlinear Vibrations in Mechanical and Electrical Systems*, volume 37 of *Wiley Classics Library*. Wiley Interscience, 1992.

[13] S.H. Strogatz. *Nonlinear Dynamics and Chaos*. Westview Press, 1994.